2004). Moreover, the NS3–4A complex was shown to suppress beta interferon (IFN-β) induction by inhibiting retinoic acid-inducible gene I-mediated activation of IFN regulatory factor 3, counteracting innate immune responses to help establish persistent HCV infection (Foy *et al.*, 2003, 2005; Breiman *et al.*, 2005).

The tumour-suppressor protein p53 functions principally to control cell-cycle arrest and apoptosis upon various cellular stresses, ensuring completion of DNA repair and the integrity of the genome (Levine, 1997). It has been documented that oncogenic viral proteins, such as papillomavirus E6 (Münger & Howley, 2002; Longworth & Laimins, 2004), adenovirus E1B 55K (Martin & Berk, 1998), simian virus 40 large T antigen (Sheppard *et al.*, 1999) and hepatitis B virus X protein (Truant *et al.*, 1995), inhibit p53-mediated apoptosis via interacting with p53. In the case of HCV, NS5A (Lan *et al.*, 2002) and core protein (Kao *et al.*, 2004) were reported to suppress p53-dependent apoptosis. Our previous studies showed that NS3 colocalized with p53 in the nucleus (Ishido *et al.*, 1997; Muramatsu *et al.*, 1997) and that they formed a complex through an N-terminal portion of NS3 (aa 29–174) and a C-terminal portion of p53 (Ishido & Hotta, 1998). In a clinical setting, we found a strong correlation between HCC and predicted secondary structure of an N-terminal portion of NS3 (Ogata *et al.*, 2003). These observations prompted us to investigate the possible correlation between NS3 sequence diversity and p53 interaction. We report here that subcellular localization of NS3 and its interaction with p53 vary with different NS3 sequences.

METHODS

Plasmid construction. cDNA fragments encoding the N-terminal 198 residues of NS3 (NS3-N; aa 1–198) of HCV subtype 1b (HCV-1b) isolates were described previously (Ogata *et al.*, 2002, 2003). *Bam*HI and *Hin*dIII recognition sites were introduced by PCR into the 5′ and 3′ ends of the cDNAs, respectively. The cDNAs were digested with *Bam*HI and *Hin*dIII and subcloned into pcDNA3.1/*Myc*-His(−)C (Invitrogen). A single point mutation(s) was introduced into some plasmids by using a QuikChange site-directed mutagenesis kit (Stratagene). Expression plasmids for Myc-tagged full-length NS3 (NS3-Full) of different HCV isolates, MKC1a, M-H05-5, M-45, M-H17-2 and M-42, were reported elsewhere (Hidajat *et al.*, 2005). To express NS3–4A *in cis*, the corresponding region was amplified from pTMns2-5B/810-2721 (Muramatsu *et al.*, 1997) and subcloned into pcDNA3.1/*Myc*-His(−)C to generate pcDNA3.1/MKC1a/4A. Expression plasmids for chimeric NS3-Full flanked with NS4A were constructed, in which the N-terminal 355 residues were derived from M-H05-5 or M-H17-2, whereas the C-terminal 330 residues were derived from MKC1a/4A. They were designated pcDNA3.1/M-H05-5/4A and pcDNA3.1/M-H17-2/4A. The NS3 sequences were subcloned also into pSG5 (Stratagene).

An *Eco*RI fragment encoding full-length NS4A was obtained from pBSns4A (Muramatsu *et al.*, 1997) and subcloned into pcDNA3.1/*Myc*-His(−)C and pSG5. Myc-tagged NS4A was amplified from pFK5B/2884Gly (a kind gift from Dr R. Bartenschlager, University of Heidelberg, Heidelberg, Germany) and subcloned into pEF1/*Myc*-His (Invitrogen). An expression plasmid for Myc-tagged NS4B was reported elsewhere (Tanaka *et al.*, 2006). To express a polyprotein consisting of full-length NS5A and C-terminally truncated NS5B (NS5A/5BΔC; aa 1973–2720 of the entire HCV polyprotein), the corresponding region was amplified from pTMns2-5B/810-2721 (Muramatsu *et al.*, 1997) and subcloned into pTM1 (Moss *et al.*, 1990).

An *Xho*I fragment encoding full-length wild-type p53 was obtained from pBSp53/1-393 (Ishido & Hotta, 1998) and subcloned into pcDNA3.1/*Myc*-His(−)C. pSG5/p53 (Florese *et al.*, 2002) was also used.

All of the plasmid constructs were verified for the correct sequence by DNA sequencing.

Cell culture and protein expression. Huh-7 and HeLa cells were cultured in Dulbecco's modified Eagle's medium supplemented with 10 % fetal calf serum. For protein expression, cells were infected with a recombinant vaccinia virus expressing T7 RNA polymerase (vTF7-3) (Fuerst *et al.*, 1986). After 1 h, the cells were transfected with the expression plasmids by using Lipofectin reagent (Invitrogen). After cultivation overnight, the proteins expressed in the cells were analysed by co-immunoprecipitation, immunoblot and immunofluorescence techniques, as described below. For the luciferase reporter assay, Huh-7 cells were transfected with plasmids by using Fugene 6 transfection reagent (Roche) and cultivated for 24 h before analysis.

Huh-7 cells stably harbouring an HCV subgenomic RNA replicon were prepared as described previously (Taguchi *et al.*, 2004; Hidajat *et al.*, 2005), using pFK5B/2884Gly (Lohmann *et al.*, 2001). Cured Huh-7 cells were prepared by treating the HCV replicon-harbouring cells with IFN-α (1000 IU ml^{-1}) for 1 month (Hidajat *et al.*, 2005). Full-length HCV RNA-harbouring Huh-7 cells, designated O, and IFN-cured cells, designated Oc, were described previously (Ikeda *et al.*, 2005).

Indirect immunofluorescence. Cells expressing Myc-tagged NS3 were fixed with methanol at −20 °C for 20 min and incubated with an anti-Myc mouse mAb (9E10; Santa Cruz Biotech) for 1 h at room temperature. In some experiments, an anti-NS3 mouse mAb (4A-3; a kind gift from Dr I. Fuke, Research Foundation for Microbial Diseases, Osaka University, Kagawa, Japan) was used to detect NS3-Full. An anti-haemagglutinin (HA) mouse mAb (HA.11; Covance Inc.) served as a control IgG. After being washed with PBS, the cells were incubated with fluorescein isothiocyanate-conjugated goat anti-mouse IgG (MBL) and observed under a laser-scanning confocal microscope (LSM510 version 3.0; Carl Zeiss).

Immunoprecipitation and immunoblotting. Cells expressing NS3 (Myc-tagged or untagged) and p53 were lysed in a stringent RIPA buffer containing 10 mM Tris/HCl (pH 7·5), 150 mM NaCl, 1 mM EDTA, 0·1 % SDS, 1 % NP-40, 0·1 % sodium deoxycholate and protease inhibitor cocktail (Roche) for 30 min on ice. The cell lysates were centrifuged and the supernatants were cleared by mixing with 0·25 μg normal rabbit IgG (Santa Cruz Biotech) and 15 μl protein A–Sepharose beads (Amersham Biosciences) at 4 °C for 30 min on a rotator to reduce non-specific precipitation. The cleared lysates were incubated with anti-p53 rabbit polyclonal antibody (FL-393; Santa Cruz Biotech) at 4 °C for 1 h and subsequently with 15 μl protein A–Sepharose beads for another 1 h. The beads were washed six times with RIPA buffer and the immunoprecipitates were separated by SDS-PAGE and analysed by immunoblotting (see below). To analyse the interaction of NS3 expressed in the context of HCV RNA replication with p53, the HCV subgenomic or full-length RNA replicon-harbouring cells were lysed in a mild RIPA buffer without 0·1 % SDS and 0·1 % sodium deoxycholate. The lysates were subjected to immunoprecipitation analysis in the same way as described above, except that the beads were washed with PBS instead of RIPA buffer. Anti-FLAG rabbit polyclonal antibody (Sigma) served as a control.

Immunoblot analysis was performed as described previously (Hidajat *et al.*, 2005). Mouse mAbs against Myc (9E10), NS3, NS4A (S4-13; a kind gift from Dr I. Fuke) and p53 (Ab-1; Calbiochem) were used as primary antibodies and peroxidase-labelled goat anti-mouse IgG (MBL) as a secondary antibody. The protein bands were visualized by an enhanced chemiluminescence method (ECL; Amersham Biosciences) and the intensity of the bands was quantified by using NIH Image 1.61.

Luciferase reporter assay. p53-Luc (Stratagene), which contains the *Photinus pyralis* (firefly) luciferase reporter gene driven by a basic promoter element plus an inducible *cis*-enhancer element, containing 14 repeats of the p53-binding sequence (TGCCTGGACTTGCCTGG), was used as a reporter plasmid. pRL-SV40 (Promega), which expresses *Renilla* luciferase, was used as a control plasmid to check transfection efficiency. Huh-7 cells prepared in a 24-well tissue-culture plate were transfected transiently with p53-Luc (10 ng), pRL-SV40 (1 ng), pSG5/p53 (5 ng) and pSG5/NS3-N or pSG5/NS3-Full (250 ng) in the absence or presence of pSG5/NS4A (75 ng). After 24 h, the cells were harvested and a luciferase assay was performed by using the Dual-Luciferase Reporter Assay system (Promega), as described previously (Kadoya *et al.*, 2005). Firefly and *Renilla* luciferase activities were measured by using a Luminescencer-JNR AB-2100 (Atto). Firefly luciferase activity was normalized to *Renilla* luciferase activity for each sample.

NS3 serine protease activity. HeLa cells transiently coexpressing NS5A/5BΔC and Myc-tagged NS3 were lysed in gel-loading buffer containing 50 mM Tris/HCl (pH 6·8), 5 % 2-mercaptoethanol, 2 % SDS, 0·1 % bromophenol blue and 10 % glycerol. The lysates were separated by SDS-PAGE and analysed by immunoblotting using anti-NS5A (8926; a kind gift from Dr I. Fuke) and anti-Myc antibodies (9E10). Intensity of the bands corresponding to the cleaved NS5A and the uncleaved NS5A/5BΔC was measured. Arbitrary units of serine protease activity of each NS3 were calculated by the following formula: protease activity (arbitrary units) = NS5A/(NS5A/5BΔC + NS5A).

RESULTS

NS3-N sequences of different HCV-1b isolates exhibit distinct subcellular-localization patterns in a sequence-dependent manner

We first examined the subcellular localization of NS3-N in HeLa cells. As shown in Fig. 1(a), we noticed three distinct patterns of NS3-N localization: (i) dot-like staining in both the cytoplasm and the nucleus, (ii) diffuse staining predominantly in the cytoplasm and (iii) a mixed pattern of the former two. Of the 29 HCV-1b isolates tested, 15 (52 %) exhibited exclusively the dot-like staining, nine (31 %) the diffuse staining and the remaining five (17 %) the mixed pattern. The subcellular-localization patterns of four NS3-N sequences each from the dot-like, diffuse and mixed staining groups are also shown in Supplementary Fig. S1 (available in JGV Online). Similar results were obtained when NS3-N sequences were expressed in Huh-7 cells (data not shown), suggesting that the distinct localization patterns among different NS3 sequences are not restricted to a particular cell line.

In order to see which amino acid residue(s) affected the subcellular localization of NS3, we determined the sequences of all 29 isolates. Some of the sequences showing the typical localization patterns, along with a standard sequence, are shown in Fig. 1(b). For more information, the sequences of all 29 isolates are shown in Supplementary Fig. S2 (available in JGV Online). We did not find any common amino acid residue(s) that was/were associated with a particular localization pattern. We noticed, however, that a substitution at position 17 or 18 (Ile to Val) was observed with some NS3 sequences of the dot-like pattern, but not with any NS3 sequences of the other localization patterns. Also, a substitution(s) at positions 150–153 (Val to Ala, Ile to Val) appeared to be more frequent in NS3 sequences of the dot-like pattern. To examine the possible importance of those substitutions, we introduced a point mutation(s) to some NS3-N of the dot-like pattern (Fig. 1c). Introduction of two point mutations at positions 18 and 153 into NS3-N of isolate H05-5 did not alter the localization pattern. However, introduction of an additional two point mutations at positions 80 and 122 altered the localization pattern significantly, with the majority of the cells exhibiting the typical diffuse staining. Similarly, introduction of two mutations at positions 17 and 86, but not of either one alone, into NS3-N of isolate 45 altered the localization pattern from dot-like to diffuse staining. As for isolate 63, a single point mutation at position 150 alone was enough to change the localization pattern of NS3-N. These results suggest that residues at positions 17 or 18, 80–86 and/or 150–153 play an important role in determining the localization pattern of some, but not all, NS3 sequences.

NS3-N binds to p53 and inhibits its *trans*-activating activity in an NS3 sequence-dependent manner

We previously reported that a region near the N terminus of NS3 (aa 29–174) was involved in complex formation with p53 (Ishido & Hotta, 1998). In this study, we examined whether interaction between NS3-N and p53 differs with different NS3-N sequences. We selected two NS3-N sequences each from the dot-like (H05-5 and 45) and diffuse (H17-2 and 42) staining groups. Co-immunoprecipitation analysis demonstrated that NS3-N of isolate H05-5 interacted with p53 most strongly, followed by that of isolate 45, both in the absence (Fig. 2a) and the presence (Fig. 2b) of NS4A. On the other hand, NS3-N of the diffuse-staining group interacted only weakly with p53. The specificity of the interaction between NS3-N and p53 was confirmed by a control experiment, in which neither NS4A nor NS4B bound to p53 under the same experimental conditions (Fig. 2c, left and centre panels). The specificity of the NS3–p53 interaction was also secured by another control experiment using an irrelevant (anti-FLAG) antibody (Fig. 2c, right panel).

Next, we examined the possible effect of NS3-N on p53 function. The plasmid p53-Luc harbours 14 copies of p53-responsive elements and a minimum promoter upstream of a luciferase gene, and is used to monitor p53-dependent transcriptional activity. Interestingly, NS3-N of H05-5 and that of isolate 45 inhibited p53-dependent transcription of the luciferase gene strongly and moderately, respectively

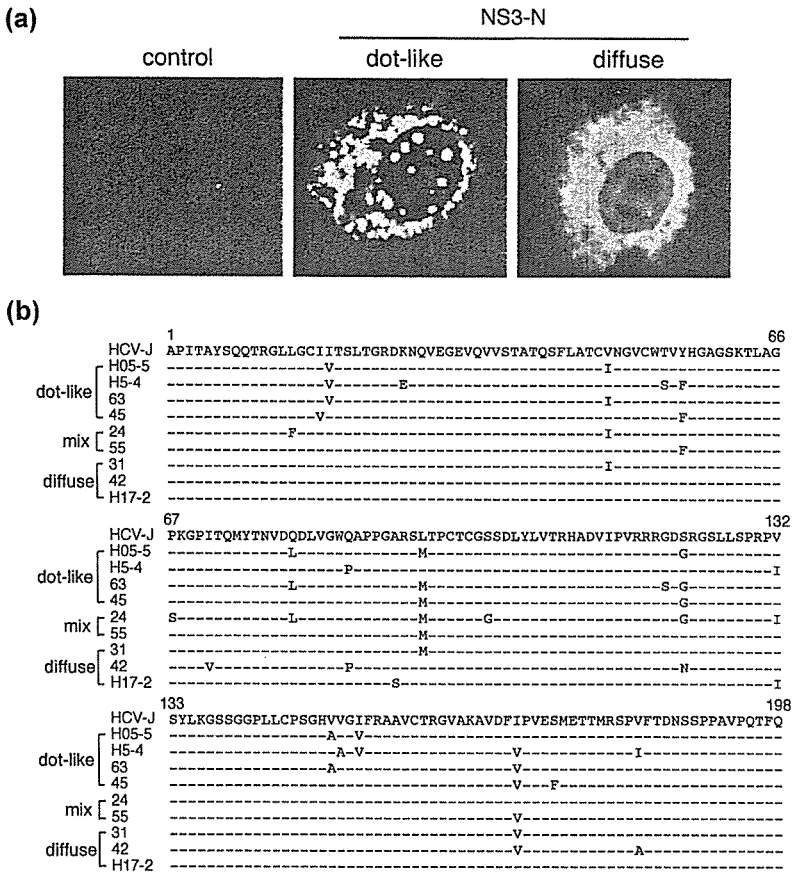

Fig. 1. Distinct subcellular-localization patterns of NS3-N of different HCV-1b isolates and the alignment of their sequences. (a) NS3-N was expressed in HeLa cells using a vaccinia virus–T7 hybrid expression method. Typical immunofluorescence images of the dot-like (middle panel) and diffuse (right panel) localization patterns of NS3-N of isolates H05-5 and H17-2, respectively, are shown. As a control, cells expressing NS3-N of H05-5 (left panel) were stained with an irrelevant (anti-HA) antibody. (b) Sequence alignment of representative sequences of each of the staining groups along with a standard sequence of the HCV-J strain (top). Dashes indicate residues identical to those of HCV-J. The numbers along the sequence indicate amino acid positions. (c) Identification of residues that alter the localization patterns of NS3-N of the isolates H05-5, 45 and 63. Substituted residues at the indicated positions are shown.

(Fig. 2d). On the other hand, no inhibition was observed with NS3-N of isolate 42 and even a slight increase in p53-dependent transcription was observed with NS3-N of H17-2.

NS3 forms a stable complex with its cofactor NS4A, which may counteract the NS3-mediated inhibitory action of p53-dependent transcription. In fact, we observed that inhibition of the p53-dependent transcription by NS3-N of the H05-5 isolate was alleviated to some extent, but not completely, by coexpression of NS4A (Fig. 2e).

To further test the possibility that the alteration in the localization pattern of NS3-N affects its interaction with p53, we compared NS3-N of H05-5 with its point mutant H05-5/mut (Fig. 1c) in terms of their p53-binding abilities and inhibitory effects on p53-dependent transcription. The result obtained demonstrated that NS3-N of H05-5/mut, which showed diffuse localization, had weaker p53-binding capacity (Fig. 3a) and exerted weaker inhibition on p53-dependent transcription (Fig. 3b) compared with NS3-N of the parental H05-5, showing the dot-like localization. Similar results were obtained with isolates 45 and 63 and their point mutants (data not shown). Our results thus suggest that NS3-N of the dot-like localization pattern interacts with p53 more strongly and inhibits p53-mediated transcriptional activation more efficiently than that of the diffuse localization.

NS3-Full sequences exhibit the same subcellular-localization patterns as those of NS3-N sequences derived from the same isolates and interact differentially with NS4A and p53 in an NS3 sequence-dependent manner

As shown above, NS3-N exhibited a distinct subcellular-localization pattern in a sequence-dependent manner when expressed alone (see Fig. 1). Moreover, we have reported that NS3, either NS3-N or NS3-Full, enters the nucleus when

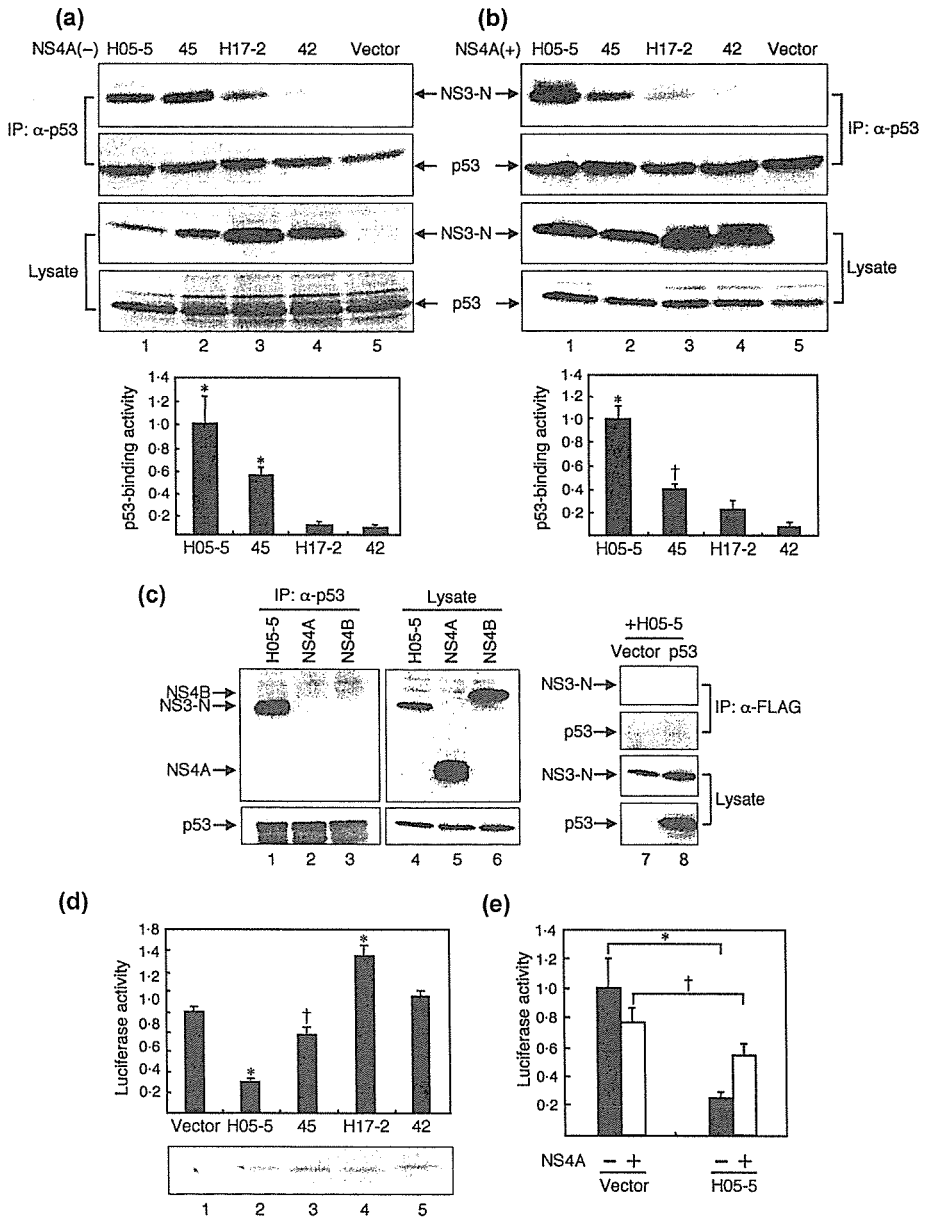

Fig. 2. Physical and functional interactions between NS3-N and p53 in an NS3 sequence-dependent manner. NS3-N and p53 were coexpressed in the absence (a) and presence (b) of NS4A. Cells that did not express NS3-N served as a control. Cell lysates were immunoprecipitated by using an anti-p53 antibody and probed by immunoblotting using an anti-Myc antibody to detect NS3-N (top row). Efficient immunoprecipitation of p53 was verified (second row). Lysates were probed directly (without being immunoprecipitated with anti-p53 antibody) with anti-Myc and anti-p53 antibodies, respectively, to verify comparable expression levels of NS3-N (third row) and p53 (bottom row). The intensity of the bands for NS3-N co-immunoprecipitated with p53 was quantified and normalized to the expression levels of NS3-N in the lysates. Filled columns and bars represent mean ± SD obtained from three independent experiments. The p53-binding intensity of NS3-N of the isolate H05-5 was expressed as 1·0. *$P<0·01$; †$P<0·05$, compared with isolate 42. (c) Cells expressing Myc-tagged H05-5, NS4A or NS4B together with p53 were analysed by immunoprecipitation using an anti-p53 antibody (left). Lysates were probed directly with anti-Myc and anti-p53 antibodies, respectively (middle). Cells expressing Myc-tagged H05-5 with or without p53 were analysed by immunoprecipitation using an irrelevant (anti-FLAG) antibody (right). (d) Inhibition of p53-dependent transcription by NS3-N in an NS3 sequence-dependent manner. pSG5-based NS3-N expression plasmids were each co-transfected with pSG5/p53, p53-Luc and pRL-SV40 in Huh-7 cells and cultivated for 24 h. Firefly luciferase activity was measured and normalized to *Renilla* luciferase activity. The luciferase activity in the control cells without NS3-N expression was expressed arbitrarily as 1·0. Results are shown as mean ± SD from three independent experiments. *$P<0·01$; †$P<0·05$, compared with the control. Expression levels of NS3-N in the cells are shown at the bottom. (e) Inhibition of p53-dependent transcription by NS3-N of H05-5 in the absence (filled bars) and presence (open bars) of NS4A. Results are shown as mean ± SD from three independent experiments. *$P<0·01$; †$P<0·05$, compared with the control.

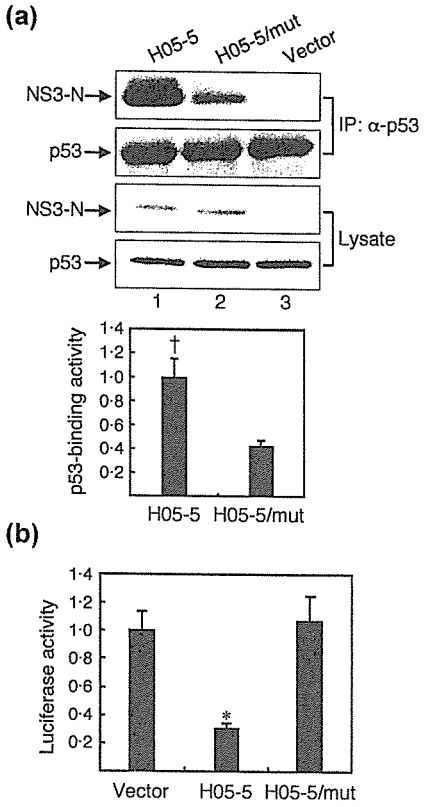

Fig. 3. Comparison between NS3-N of the isolate H05-5 and its point mutant H05-5/mut in their capacity to interact with p53. (a) Physical interaction with p53 was analysed as described in the legend to Fig. 2(a). Filled columns and bars represent mean ± SD obtained from three independent experiments. The p53-binding intensity of NS3-N of H05-5 was expressed as 1·0. †$P<0·05$. (b) Functional interaction with p53 was analysed as described in the legend to Fig. 2(c). Results are shown as mean ± SD from three independent experiments. *$P<0·01$ compared with H05-5/mut.

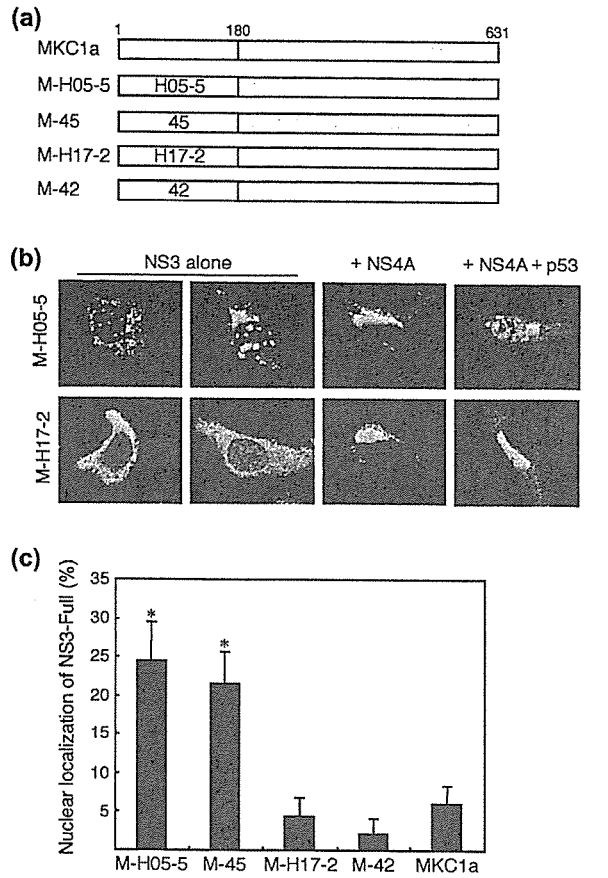

Fig. 4. Subcellular localization of NS3-Full in the presence and absence of NS4A and p53. (a) Schematic representation of NS3-Full of different sequences. The N-terminal 180 residues are derived from clinical isolates (H05-5, H17-2, 42 and 45) and the C-terminal 451 residues from the parental MKC1a strain. (b) Subcellular localization of M-H05-5 (upper) and M-H17-2 (lower) when expressed alone, when coexpressed with NS4A and when coexpressed with NS4A and p53. The cells were stained with either anti-NS3 (left panels) or anti-Myc antibody (left-middle, right-middle and right panels). (c) Percentage of cells with nuclear accumulation of NS3-Full when coexpressed with NS4A and p53. *$P<0·01$ compared with M-42.

coexpressed with p53 and that the p53-mediated nuclear localization of NS3 is inhibited by NS4A in an NS3 sequence-dependent manner (Muramatsu *et al.*, 1997). Therefore, we examined the subcellular-localization patterns of NS3-Full of different sequences, both when expressed alone and when coexpressed with p53 and/or NS4A. The NS3-Full sequences tested differ from each other only in the N-terminal 180 residues that are derived from the clinical isolates, with the C-terminal 451 residues being shared among all the strains tested (Fig. 4a; Hidajat *et al.*, 2005). When expressed alone, NS3-Full of all four strains exhibited the same subcellular-localization patterns as those of NS3-N of the same strains (Fig. 4b; data not shown for M-45 and M-42). When coexpressed with NS4A, NS3-Full was localized in the cytoplasm, especially in perinuclear regions, regardless of the strain tested. Interestingly, when p53 was additionally coexpressed with NS4A, NS3-Full of the dot-like type (M-H05-5 and M-45) showed an increased tendency to accumulate in the nucleus together with p53 (Fig. 4b), with nearly 25 % of the cells exhibiting nuclear localization of NS3 (Fig. 4c). Concomitant expression of NS4A in the cytoplasm of the same cells was confirmed by double-staining immunofluorescence analysis (data not shown), the result being consistent with our previous observation (Ishido *et al.*, 1997). On the other hand, NS3-Full of the diffuse type (M-H17-2, M-42 and MKC1a) was localized almost exclusively in the cytoplasm together with NS4A. Similar results were obtained when NS3-N sequences of different isolates were coexpressed with p53 and/or NS4A (data not shown).

We then tested complex formation between NS3-Full of the five different sequences and p53. The results demonstrated clearly that NS3-Full of the dot-like type (M-H05-5 and

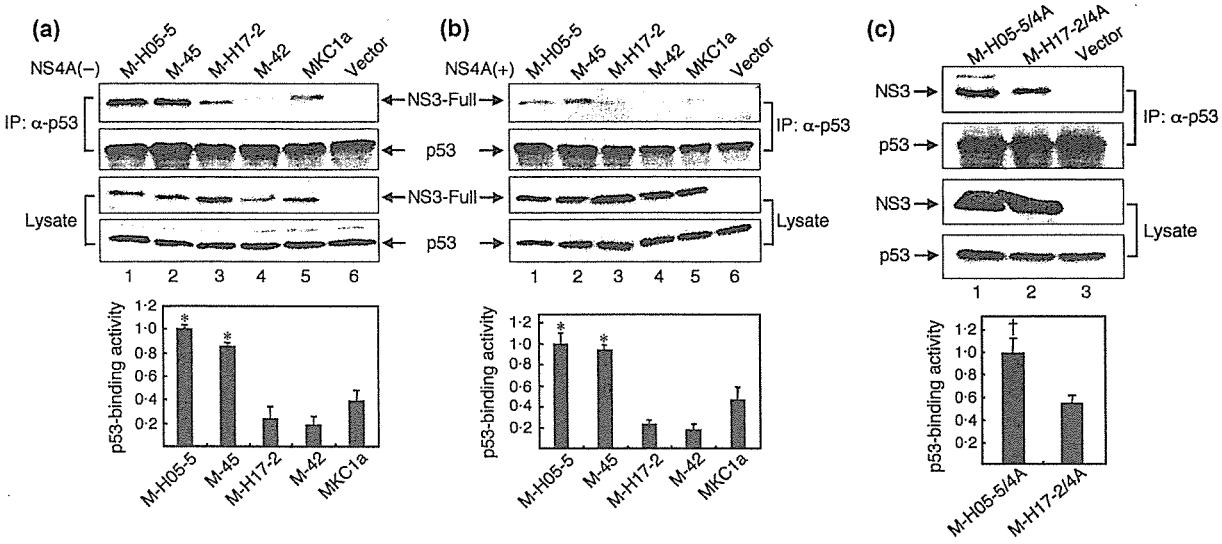

Fig. 5. Physical interaction between NS3-Full and p53 in an NS3 sequence-dependent manner. NS3-Full of different strains in the absence (a) and presence of NS4A coexpression *in trans* (b) were analysed as described in the legend to Fig. 2(a). Filled columns and bars represent mean ± SD obtained from three independent experiments. The p53-binding intensity of M-H05-5 was expressed as 1·0. *$P<0{\cdot}01$ compared with M-42. (c) M-H05-5/4A and M-H17-2/4A (NS3–4A coexpression *in cis*) were analysed as described in the legend to Fig. 2(a), except that anti-NS3 antibody was used instead of anti-Myc antibody. Filled columns and bars represent mean ± SD obtained from three independent experiments. The p53-binding intensity of M-H05-5/4A was expressed as 1·0. †$P<0{\cdot}05$ compared with M-H17-2/4A.

M-45) interacted with p53 more strongly than that of the diffuse type (M-H17-2, M-42 and MKC1a), both in the absence and presence of NS4A (Fig. 5a, b). In this connection, it should be noted that the interaction between NS3-Full and p53 was weaker in the presence of NS4A than in its absence. We also examined the interaction of NS3 with p53 when full-length NS3–4A was expressed *in cis*, where NS3–4A complex formation occurs more efficiently than *in trans*. The results demonstrated that M-H05-5/4A interacted with p53 more strongly than did M-H17-2/4A (Fig. 5c), again suggesting NS3 sequence-dependent interaction with p53.

NS3 binds to p53 and inhibits its *trans*-activating activity in HCV RNA replicon-harbouring cells

In order to determine whether NS3 expressed in the context of HCV replication interacted with p53, we used Huh-7 cells harbouring an HCV subgenomic RNA replicon and examined physical and functional interactions between NS3 and p53. Co-immunoprecipitation analysis revealed that NS3 interacted physically with p53 in HCV subgenomic RNA replicon-harbouring cells, albeit with much lower efficiency than in the plasmid-based expression system (Fig. 6a). We also used the full-length HCV RNA replicon, whose NS3 is detected more strongly than that of the subgenomic RNA replicon by the anti-NS3 mAb used in this study. The result demonstrated that NS3 expressed in the context of HCV RNA replication interacted efficiently with p53, irrespective of whether p53 was expressed ectopically or endogenously (Fig. 6b). The specificity of the interaction between NS3 and p53 was confirmed by the lack of interaction between NS4A and p53 in HCV subgenomic RNA-harbouring cells (Fig. 6c). Next, we compared *trans*-activating activity of p53 between HCV RNA replicon-harbouring cells and the HCV-negative controls (parental and cured Huh-7 cells). We observed that p53-dependent transcription was suppressed significantly in cells harbouring an HCV RNA replicon, either subgenomic or full-length, compared with the parental and cured Huh-7 cells (Fig. 6d, e). These results suggest collectively that NS3 expressed in the context of HCV replication inhibits p53 function.

Serine protease activity of NS3-Full in the absence and presence of NS4A

The N-terminal portion of NS3 possesses a serine protease activity that can cleave the NS5A/5B junction even in the absence of NS4A (Lin *et al.*, 1994). By using NS5A/5BΔC as a substrate, we compared the serine protease activities of NS3-Full of different subcellular-localization patterns. A tendency was noted that, in the absence of NS4A, NS3-Full of the dot-like type showed slightly weaker protease activity than that of the diffuse type (Fig. 7). This difference might be attributable, at least partly, to the fact that NS5A/5BΔC was localized diffusely in the cytoplasm (Kim *et al.*, 1999; Mottola *et al.*, 2002; data not shown) and, therefore, could be recognized more easily by NS3 of the same localization pattern than by NS3 of the other type. In the presence of

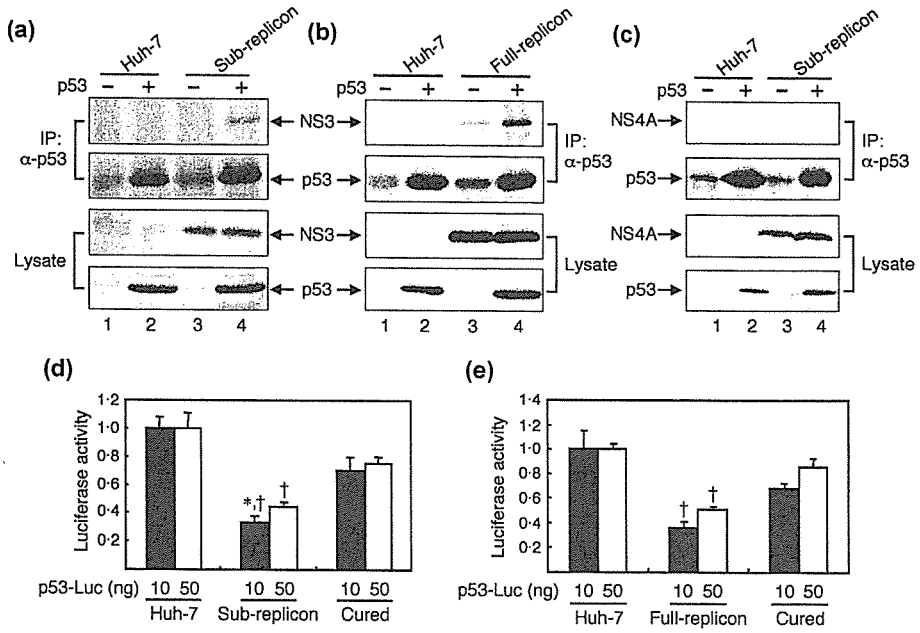

Fig. 6. Physical and functional interactions between NS3 and p53 in HCV RNA replicon-harbouring cells. p53 was expressed ectopically in Huh-7 cells harbouring either HCV subgenomic (a) or full-length (b) RNA replicon and the parental Huh-7 cells by using a vaccinia virus–T7 hybrid expression method. Cell lysates were analysed as described in Methods. (c) The lack of interaction between NS4A and p53 in HCV subgenomic RNA replicon-harbouring Huh-7 cells was confirmed. Inhibition of p53-dependent transcription in Huh-7 cells harbouring either HCV subgenomic (d) or full-length (e) RNA replicon. Cells were co-transfected with p53-Luc (10 and 50 ng, filled and open bars, respectively), pSG5/p53 (10 ng) and pRL-SV40 (1 ng) as an internal control. After 24 h, firefly luciferase activity was measured and normalized to *Renilla* luciferase activity. Luciferase activities in the parental Huh-7 cells were expressed arbitrarily as 1·0. Cured cells also served as a control. Results are shown as mean ± SD from three independent experiments. $*P<0{\cdot}01$; $\dagger P<0{\cdot}05$, compared with the parental and cured Huh-7 cells.

NS4A, on the other hand, all of the NS3-Full sequences, which accumulated at a perinuclear region of the cytoplasm (see Fig. 4b), exhibited an enhanced and comparable degree of serine protease activity among the five strains (Fig. 7). Similar results were obtained when Huh-7 cells were used instead of HeLa cells (data not shown).

DISCUSSION

In the present study we demonstrated that, when expressed alone, NS3 of HCV-1b isolates, either NS3-N or NS3-Full, exhibited distinct subcellular-localization patterns, i.e. (i) dot-like staining both in the cytoplasm and the nucleus, (ii) diffuse staining predominantly in the cytoplasm and (iii) a mixed type, in a sequence-dependent manner (Figs 1 and 4). Although no significant correlation has been observed so far between the localization patterns of NS3 and the HCC status of the patients, it was interesting to find that NS3-N and NS3-Full of the dot-like staining pattern interacted with p53 more strongly than that of the diffuse-staining pattern (Figs 2a, 3a and 5a). Similar results were obtained when NS3 was coexpressed with NS4A (Figs 2b, 5b and 5c). We also observed that both NS3-N and NS3-Full of the dot-like staining pattern, but not those of the diffuse pattern, were more prone to colocalize with p53 in the nucleus even in the presence of NS4A (Fig. 4). Luciferase reporter analysis demonstrated that NS3-N of the dot-like type, but not that of the diffuse type, suppressed p53-dependent transcriptional activation significantly (Figs 2d and 3b).

When cells are exposed to a variety of stresses, p53 is induced to accumulate in the nucleus, where it functions as a transcription factor for cell-cycle regulators such as p21 (Levine, 1997). Our present results demonstrated that NS3-N of isolate H05-5 inhibited p53-dependent transcription of a reporter gene strongly (Figs 2d and 3b). We need to assess two possible mechanisms for the NS3-N-mediated p53 inhibition: NS3 might inhibit either p53 expression or p53 function itself. Our results showed that p53 expression levels were not altered significantly by NS3-N, irrespective of the localization patterns (Fig. 2a, b, bottom). Similar results that neither p53 mRNA nor protein levels were downregulated by NS3 were reported by Kwun *et al.* (2001). Overexpression of p53 was even observed in hepatocytes of some, if not all, HCV-infected patients (Loguercio *et al.*, 2003). It is likely, therefore, that NS3-N inhibits p53 function by interacting with it physically.

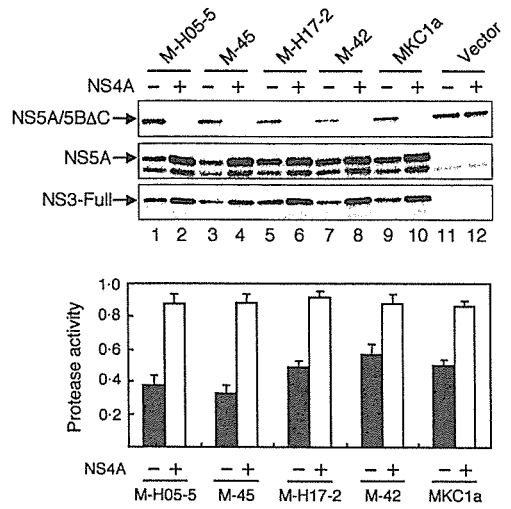

Fig. 7. Serine protease activity of NS3-Full in the absence and presence of NS4A. NS3-Full of different strains and NS5A/5BΔC were coexpressed in HeLa cells without (lanes with odd numbers) or with (lanes with even numbers) NS4A using a vaccinia virus–T7 hybrid expression method. Cell lysates were subjected to immunoblotting using anti-NS5A or anti-Myc antibody to detect NS5A/5BΔC (top), NS5A (middle) and NS3 (bottom). The intensity of the bands was quantified and arbitrary units of serine protease activity were calculated as described in Methods. Serine protease activities of NS3-Full in the absence (filled bars) and presence (open bars) of NS4A obtained from three independent experiments are shown.

We previously reported that a region of p53 near the C terminus (aa 301–360) was involved in complex formation with NS3 (Ishido & Hotta, 1998). This region includes the p53 oligomerization domain (aa 324–355) (Levine, 1997). It is known that the p53 tetramer binds to the p53-response element on promoter sequences most efficiently and, therefore, is most effective in *trans*-activation of its target genes (McLure & Lee, 1998; Weinberg *et al.*, 2004). Recently, it was reported that proteins of the S100 family disrupted p53 tetramerization via binding to its tetramerization domain (Fernandez-Fernandez *et al.*, 2005). Therefore, it is reasonable to assume that interaction of NS3-N with p53 interferes with its tetramer formation and DNA binding, thereby inhibiting p53-dependent transcriptional activation. It was also reported that a C-terminal portion of p53 (aa 364–393) negatively regulated its DNA-binding capacity (Müller-Tiemann *et al.*, 1998) and that the 14-3-3 proteins could associate with this region to counteract the negative regulation, which resulted in increased DNA binding of p53 (Waterman *et al.*, 1998). It is tempting to speculate that, by binding to a nearby region of p53, NS3-N may impair the association of 14-3-3 proteins with p53, which results in comparably decreased DNA binding of p53. Moreover, p53 is subject to post-translational modifications, including phosphorylation and acetylation, that affect p53 function (Appella & Anderson, 2001). Further study is needed to determine whether such p53 modification status is affected, either directly or indirectly, by NS3-N.

Consistent with the results obtained from transient-expression experiments, physical interaction between NS3 and p53 was also observed in Huh-7 cells harbouring either an HCV subgenomic or full-length RNA replicon, albeit to a smaller extent than in the transient-expression system (Fig. 6). It should be noted that NS3 expressed by the full-length RNA replicon is detected more strongly by the anti-NS3 antibody used in this study than that of the subgenomic RNA replicon. In HCV RNA replicon-harbouring cells, the HCV non-structural proteins are incorporated into the HCV RNA replication complex and, therefore, it is conceivable that only a minor fraction of NS3 is available for the interaction with p53. Nevertheless, p53-mediated transcriptional activation was suppressed significantly in HCV RNA replicon-harbouring cells compared with the controls (Fig. 6d, e). We must consider the possibility that not only NS3, but also other HCV proteins, are involved in the observed p53 inhibition. In fact, interaction between NS5A and p53 has been reported (Lan *et al.*, 2002; Qadri *et al.*, 2002).

In conclusion, our present results have demonstrated that NS3 of HCV-1b can be divided into three groups based on the subcellular-localization patterns and that NS3 of the dot-like localization pattern interacts with, and inhibits the function of, the tumour suppressor p53 more strongly than that of the diffuse type. The observed difference may account, at least partly, for a different degree of the oncogenic capacity of different HCV-1b isolates.

ACKNOWLEDGEMENTS

The authors are grateful to Dr I. Fuke, Research Institute for Microbial Diseases, Kan-Onji Branch, Kagawa, Japan, for providing anti-NS3, anti-NS4A and anti-NS5A mAbs. Thanks are also due to Dr R. Bartenschlager (University of Heidelberg, Heidelberg, Germany) for providing an HCV subgenomic RNA replicon (pFK5B/2884Gly). This study was supported in part by Grants-in-Aid for Scientific Research from the Ministry of Education, Culture, Sports, Science and Technology, the Japan Society for the Promotion of Science and the Ministry of Health, Labour and Welfare, Japan. This study was also carried out as part of the 21COE Program at Kobe University Graduate School of Medicine.

REFERENCES

Appella, E. & Anderson, C. W. (2001). Post-translational modifications and activation of p53 by genotoxic stresses. *Eur J Biochem* **268**, 2764–2772.

Breiman, A., Grandvaux, N., Lin, R., Ottone, C., Akira, S., Yoneyama, M., Fujita, T., Hiscott, J. & Meurs, E. F. (2005). Inhibition of RIG-I-dependent signaling to the interferon pathway during hepatitis C virus expression and restoration of signaling by IKKε. *J Virol* **79**, 3969–3978.

Cheng, P.-L., Chang, M.-H., Chao, C.-H. & Wu Lee, Y.-H. (2004). Hepatitis C viral proteins interact with Smad3 and differentially regulate TGF-β/Smad3-mediated transcriptional activation. *Oncogene* **23**, 7821–7838.

Fernandez-Fernandez, M. R., Veprintsev, D. B. & Fersht, A. R. (2005). Proteins of the S100 family regulate the oligomerization of p53 tumor suppressor. *Proc Natl Acad Sci U S A* **102**, 4735–4740.

Florese, R. H., Nagano-Fujii, M., Iwanaga, Y., Hidajat, R. & Hotta, H. (2002). Inhibition of protein synthesis by the nonstructural proteins NS4A and NS4B of hepatitis C virus. *Virus Res* **90**, 119–131.

Foy, E., Li, K., Wang, C., Sumpter, R., Jr, Ikeda, M., Lemon, S. M. & Gale, M., Jr (2003). Regulation of interferon regulatory factor-3 by the hepatitis C virus serine protease. *Science* **300**, 1145–1148.

Foy, E., Li, K., Sumpter, R., Jr & 8 other authors (2005). Control of antiviral defenses through hepatitis C virus disruption of retinoic acid-inducible gene-I signaling. *Proc Natl Acad Sci U S A* **102**, 2986–2991.

Fuerst, T. R., Niles, E. G., Studier, F. W. & Moss, B. (1986). Eukaryotic transient-expression system based on recombinant vaccinia virus that synthesizes bacteriophage T7 RNA polymerase. *Proc Natl Acad Sci U S A* **83**, 8122–8126.

Fujita, T., Ishido, S., Muramatsu, S., Itoh, M. & Hotta, H. (1996). Suppression of actinomycin D-induced apoptosis by the NS3 protein of hepatitis C virus. *Biochem Biophys Res Commun* **229**, 825–831.

Hidajat, R., Nagano-Fujii, M., Deng, L., Tanaka, M., Takigawa, Y., Kitazawa, S. & Hotta, H. (2005). Hepatitis C virus NS3 protein interacts with ELKS-δ and ELKS-α, members of a novel protein family involved in intracellular transport and secretory pathways. *J Gen Virol* **86**, 2197–2208.

Ikeda, M., Abe, K., Dansako, H., Nakamura, T., Naka, K. & Kato, N. (2005). Efficient replication of a full-length hepatitis C virus genome, strain O, in cell culture, and development of a luciferase reporter system. *Biochem Biophys Res Commun* **329**, 1350–1359.

Ishido, S. & Hotta, H. (1998). Complex formation of the non-structural protein 3 of hepatitis C virus with the p53 tumor suppressor. *FEBS Lett* **438**, 258–262.

Ishido, S., Muramatsu, S., Fujita, T., Iwanaga, Y., Tong, W.-Y., Katayama, Y., Itoh, M. & Hotta, H. (1997). Wild-type, but not mutant-type, p53 enhances nuclear accumulation of the NS3 protein of hepatitis C virus. *Biochem Biophys Res Commun* **230**, 431–436.

Kadoya, H., Nagano-Fujii, M., Deng, L., Nakazono, N. & Hotta, H. (2005). Nonstructural proteins 4A and 4B of hepatitis C virus transactivate the interleukin 8 promoter. *Microbiol Immunol* **49**, 265–273.

Kao, C.-F., Chen, S.-Y., Chen, J.-Y. & Wu Lee, Y.-H. (2004). Modulation of p53 transcription regulatory activity and post-translational modification by hepatitis C virus core protein. *Oncogene* **23**, 2472–2483.

Kim, D. W., Gwack, Y., Han, J. H. & Choe, J. (1995). C-terminal domain of the hepatitis C virus NS3 protein contains an RNA helicase activity. *Biochem Biophys Res Commun* **215**, 160–166.

Kim, J.-E., Song, W. K., Chung, K. M., Back, S. H. & Jang, S. K. (1999). Subcellular localization of hepatitis C viral proteins in mammalian cells. *Arch Virol* **144**, 329–343.

Kwun, H. J., Jung, E. Y., Ahn, J. Y., Lee, M. N. & Jang, K. L. (2001). p53-dependent transcriptional repression of $p21^{waf1}$ by hepatitis C virus NS3. *J Gen Virol* **82**, 2235–2241.

Lan, K.-H., Sheu, M.-L., Hwang, S.-J. & 8 other authors (2002). HCV NS5A interacts with p53 and inhibits p53-mediated apoptosis. *Oncogene* **21**, 4801–4811.

Levine, A. J. (1997). p53, the cellular gatekeeper for growth and division. *Cell* **88**, 323–331.

Lin, C., Prágai, B. M., Grakoui, A., Xu, J. & Rice, C. M. (1994). Hepatitis C virus NS3 serine proteinase: *trans*-cleavage requirements and processing kinetics. *J Virol* **68**, 8147–8157.

Loguercio, C., Cuomo, A., Tuccillo, C., Gazzerro, P., Cioffi, M., Molinari, A. M. & Del Vecchio Blanco, C. (2003). Liver p53 expression in patients with HCV-related chronic hepatitis. *J Viral Hepat* **10**, 266–270.

Lohmann, V., Körner, F., Dobierzewska, A. & Bartenschlager, R. (2001). Mutations in hepatitis C virus RNAs conferring cell culture adaptation. *J Virol* **75**, 1437–1449.

Longworth, M. S. & Laimins, L. A. (2004). Pathogenesis of human papillomaviruses in differentiating epithelia. *Microbiol Mol Biol Rev* **68**, 362–372.

Martin, M. E. D. & Berk, A. J. (1998). Adenovirus E1B 55K represses p53 activation in vitro. *J Virol* **72**, 3146–3154.

McLure, K. G. & Lee, P. W. K. (1998). How p53 binds DNA as a tetramer. *EMBO J* **17**, 3342–3350.

Moss, B., Elroy-Stein, O., Mizukami, T., Alexander, W. A. & Fuerst, T. R. (1990). New mammalian expression vectors. *Nature* **348**, 91–92.

Mottola, G., Cardinali, G., Ceccacci, A., Trozzi, C., Bartholomew, L., Torrisi, M. R., Pedrazzini, E., Bonatti, S. & Migliaccio, G. (2002). Hepatitis C virus nonstructural proteins are localized in a modified endoplasmic reticulum of cells expressing viral subgenomic replicons. *Virology* **293**, 31–43.

Müller-Tiemann, B. F., Halazonetis, T. D. & Elting, J. J. (1998). Identification of an additional negative regulatory region for p53 sequence-specific DNA binding. *Proc Natl Acad Sci U S A* **95**, 6079–6084.

Münger, K. & Howley, P. M. (2002). Human papillomavirus immortalization and transformation functions. *Virus Res* **89**, 213–228.

Muramatsu, S., Ishido, S., Fujita, T., Itoh, M. & Hotta, H. (1997). Nuclear localization of the NS3 protein of hepatitis C virus and factors affecting the localization. *J Virol* **71**, 4954–4961.

Ogata, S., Ku, Y., Yoon, S., Makino, S., Nagano-Fujii, M. & Hotta, H. (2002). Correlation between secondary structure of an amino-terminal portion of the nonstructural proteins 3 (NS3) of hepatitis C virus and development of hepatocellular carcinoma. *Microbiol Immunol* **46**, 549–554.

Ogata, S., Florese, R. H., Nagano-Fujii, M. & 7 other authors (2003). Identification of hepatitis C virus (HCV) subtype 1b strains that are highly, or only weakly, associated with hepatocellular carcinoma on the basis of the secondary structure of an amino-terminal portion of the HCV NS3 protein. *J Clin Microbiol* **41**, 2835–2841.

Qadri, I., Iwahashi, M. & Simon, F. (2002). Hepatitis C virus NS5A protein binds TBP and p53, inhibiting their DNA binding and p53 interactions with TBP and ERCC3. *Biochim Biophys Acta* **1592**, 193–204.

Reed, K. E. & Rice, C. M. (2000). Overview of hepatitis C virus genome structure, polyprotein processing, and protein properties. *Curr Top Microbiol Immunol* **242**, 55–84.

Saito, I., Miyamura, T., Ohbayashi, A. & 10 other authors (1990). Hepatitis C virus infection is associated with the development of hepatocellular carcinoma. *Proc Natl Acad Sci U S A* **87**, 6547–6549.

Sakamuro, D., Furukawa, T. & Takegami, T. (1995). Hepatitis C virus nonstructural protein NS3 transforms NIH3T3 cells. *J Virol* **69**, 3893–3896.

Sheppard, H. M., Corneillie, S. I., Espiritu, C., Gatti, A. & Liu, X. (1999). New insights into the mechanism of inhibition of p53 by simian virus 40 large T antigen. *Mol Cell Biol* **19**, 2746–2753.

Taguchi, T., Nagano-Fujii, M., Akutsu, M., Kadoya, H., Ohgimoto, S., Ishido, S. & Hotta, H. (2004). Hepatitis C virus NS5A protein interacts with 2′,5′-oligoadenylate synthetase and inhibits antiviral activity of IFN in an IFN sensitivity-determining region-independent manner. *J Gen Virol* **85**, 959–969.

Tanaka, M., Nagano-Fujii, M., Deng, L., Ishido, S., Sada, K. & Hotta, H. (2006). Single-point mutations of hepatitis C virus NS3 that impair p53 interaction and anti-apoptotic activity of NS3. *Biochem Biophys Res Commun* **340**, 792–799.

Truant, R., Antunovic, J., Greenblatt, J., Prives, C. & Cromlish, J. A. (1995). Direct interaction of the hepatitis B virus HBx protein with p53 leads to inhibition by HBx of p53 response element directed-transactivation. *J Virol* **69**, 1851–1859.

Waterman, M. J. F., Stavridi, E. S., Waterman, J. L. F. & Halazonetis, T. D. (1998). ATM-dependent activation of p53 involves dephosphorylation and association with 14-3-3 proteins. *Nat Genet* **19**, 175–178.

Weinberg, R. L., Veprintsev, D. B. & Fersht, A. R. (2004). Cooperative binding of tetrameric p53 to DNA. *J Mol Biol* **341**, 1145–1159.

Zemel, R., Gerechet, S., Greif, H. & 7 other authors (2001). Cell transformation induced by hepatitis C virus NS3 serine protease. *J Viral Hepat* **8**, 96–102.

The EMBO Journal (2006) 25, 3618–3626 | © 2006 European Molecular Biology Organization | All Rights Reserved 0261-4189/06
www.embojournal.org

THE EMBO JOURNAL

A novel mitochondrial ubiquitin ligase plays a critical role in mitochondrial dynamics

Ryo Yonashiro[1,2], Satoshi Ishido[3,*], Shinkou Kyo[2], Toshifumi Fukuda[1], Eiji Goto[2,3], Yohei Matsuki[2,3], Mari Ohmura-Hoshino[3], Kiyonao Sada[2], Hak Hotta[2], Hirohei Yamamura[2], Ryoko Inatome[1,2] and Shigeru Yanagi[1,4,*]

[1]Laboratory of Molecular Biochemistry, School of Life Science, Tokyo University of Pharmacy and Life Science, Hachioji, Tokyo, Japan, [2]Department of Genome Science, Kobe University Graduate School of Medicine, Chuo-Ku, Kobe, Japan, [3]Laboratory for Infectious Immunity, RIKEN Research Center for Allergy and Immunology, Tsurumi-ku, Yokohama, Kanagawa, Japan and [4]PRESTO, Japan Science and Technology Agency (JST), Kawaguchi, Saitama, Japan

In this study, we have identified a novel mitochondrial ubiquitin ligase, designated MITOL, which is localized in the mitochondrial outer membrane. MITOL possesses a Plant Homeo-Domain (PHD) motif responsible for E3 ubiquitin ligase activity and predicted four-transmembrane domains. MITOL displayed a rapid degradation by auto-ubiquitination activity in a PHD-dependent manner. HeLa cells stably expressing a MITOL mutant lacking ubiquitin ligase activity or MITOL-deficient cells by small interfering RNA showed an aberrant mitochondrial morphology such as fragmentation, suggesting the enhancement of mitochondrial fission by MITOL dysfunction. Indeed, a dominant-negative expression of Drp1 mutant blocked mitochondrial fragmentation induced by MITOL depletion. We found that MITOL associated with and ubiquitinated mitochondrial fission protein hFis1 and Drp1. Pulse–chase experiment showed that MITOL overexpression increased turnover of these fission proteins. In addition, overexpression phenotype of hFis1 could be reverted by MITOL co-overexpression. Our finding indicates that MITOL plays a critical role in mitochondrial dynamics through the control of mitochondrial fission proteins.

The EMBO Journal (2006) **25**, 3618–3626. doi:10.1038/sj.emboj.7601249; Published online 27 July 2006
Subject Categories: proteins
Keywords: E3 ubiquitin ligase; mitochondria; mitochondrial dynamics; mitochondrial fission

Introduction

Ubiquitination is a post-translational modification in which a small conserved peptide, ubiquitin, is appended to target proteins in the cell through a series of complex enzymatic reactions (Hershko and Ciechanover, 1992). The ubiquitin–proteasome system plays an important role in controlling the levels of various cellular proteins and regulates basic cellular processes such as cell cycle progression, signal transduction, cell transformation and immune recognition (Hershko and Ciechanover, 1998). This system is also involved in the protein quality control, which maintains the health of the cell (Sitia and Braakman, 2003).

E3 ubiquitin ligases are a large family of proteins that can be classified into three major structurally distinct types: N-end rule E3, E3 containing the HECT (Homology to E6AP C-Terminus) domain and E3 with the RING (Really Interesting New Gene) finger, including its derivatives, the U-Box and the PHD (Plant Homeo-Domain) (Jackson *et al*, 2000; Pickart, 2001; Patterson, 2002). PHD constitutes a widely distributed subfamily of zinc fingers and had been initially believed to be involved in chromatin-mediated transcriptional regulation. But recent studies have demonstrated that various proteins containing PHD function as E3 ubiquitin ligases including MEKK1 and Doa10 (Coscoy and Ganem, 2003). Subsequently, several PHD-containing viral proteins have been identified that promote immune evasion by down-regulating proteins that govern immune recognition (Ishido *et al*, 2000a). For example, Kaposi's sarcoma-associated herpesvirus encodes two proteins, MIR (modulator of immune recognition) 1 and 2, which have been shown to contain PHD and function as E3 ubiquitin ligases for immune recognition-related molecules such as MHC class I (Ishido *et al*, 2000b; Means *et al*, 2002). Thus, these viral regulators lead to ubiquitination of their targets by functioning as E3 ubiquitin ligases that require the PHD motif. We have recently demonstrated that human genome also encodes a novel PHD-containing protein that functions as an E3 ubiquitin ligase designated as c-MIR (Goto *et al*, 2003). Furthermore, in a genome screen for related mammalian proteins containing PHD like c-MIR, we discovered a novel membrane-bound E3 ubiquitin ligase designated MITOL, which is specifically localized in mitochondria.

Mitochondria are the center of cellular energy production and essential metabolic reactions, and are involved in the induction of apoptosis by release of cytochrome *c*. Mitochondria are remarkably dynamic organelles. Time-lapse microscopy of living cells reveals that mitochondria undergo constant migration and morphological changes. The mitochondrial fission and fusion machinery plays an essential role in the dynamics, division, distribution and morphology of the organelle (Yaffe, 1999; Jensen *et al*, 2000; Griparic and van der Bliek, 2001; Shaw and Nunnari, 2002). Evolutionarily conserved large GTPases Dnm1/Drp1/Dlp1 and Fzo1/mitofusin are involved in mitochondrial fission and fusion, respectively (Hales and Fuller, 1997; Hermann *et al*, 1998; Labrousse *et al*, 1999; Sesaki and Jensen, 1999). Mammalian protein hFis1 is the orthologue of the yeast Fis1p known to participate in yeast mitochondrial division (James *et al*, 2003). However, their regulatory mechanisms are largely unknown.

*Corresponding authors. S Yanagi, Laboratory of Molecular Biochemistry, School of Life Science, Tokyo University of Pharmacy and Life Science, 1432-1 Horinouchi, Hachioji, Tokyo 192-0392, Japan. Tel.: +81 42 676 7146; Fax: +81 42 676 4149; E-mail: syanagi@ls.toyaku.ac.jp or S Ishido. Tel.: +81 45 503 7022; Fax: +81 45 503 7021; E-mail: ishido@rcai.riken.jp

Received: 24 February 2006; accepted: 29 June 2006; published online: 27 July 2006

In this study, we demonstrate that MITOL is involved in the regulation of mitochondrial dynamics through the down-regulation of mitochondrial fission proteins. We discuss a crucial role of MITOL in mitochondrial biology.

Results

MITOL is a novel mitochondria-specific E3 ubiquitin ligase

In a human genome screening for MIR family, we identified a novel mitochondrial ubiquitin ligase and named it MITOL. Figure 1A shows the amino-acid sequence of MITOL. MITOL contains a PHD motif at its N-terminus and predicted four-transmembrane domains. We first examined whether PHD in MITOL exhibited E3 ubiquitin ligase activity. For this purpose, two constructs, GST-fused PHD (2–72 amino acids of MITOL) and GST-fused PHD mutant (CS mutant; C65S, C68S), which lacks Zn-binding ability, were generated. *In vitro* ubiquitination assay using lysate of rabbit reticulocytes containing E1 and E2s revealed a clear polyubiquitin signal in GST-PHD but not in GST or GST-PHD CS mutant (Figure 1B). This indicated that PHD in MITOL has an E3 ubiquitin ligase activity. Northern blot analysis showed the ubiquitous expression of MITOL in various human tissues (Figure 1C). To ascertain expression of MITOL a specific anti-MITOL antibody was raised against a peptide corresponding to amino acids 257–279 of MITOL. Western blot analysis with anti-MITOL antibody demonstrated the expression of MITOL as an ≈30 kDa band in both COS-7 and HeLa cells, but not with control, preimmune serum (Figure 1D). In addition, an enhanced MITOL signal in MITOL expression vector-transfected cells verified the specificity of this antibody and the position of MITOL protein band.

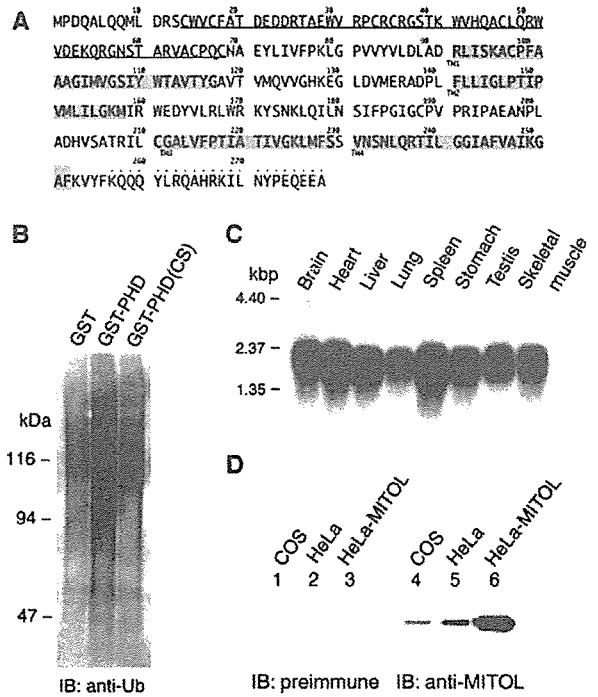

Figure 1 Identification of MITOL, a novel membrane-bound E3 ubiquitin ligase. (**A**) Amino-acid sequence of human MITOL. PHD motif and predicted four-transmembrane domains are shown by an underline and shadow lines, respectively. Anti-MITOL antibody was raised against the peptide indicated by dots above the amino acids. (**B**) E3 ubiquitin ligase activity in GST-fused MITOL-PHD, but not CS mutant (C65S, C68S). *In vitro* ubiquitin ligase assay using purified GST, GST-PHD and GST-PHD CS mutants was performed as described in Materials and methods. (**C**) Northern blot analysis of MITOL in various human tissues. A full-length human MITOL cDNA was used as a probe. (**D**) Expression of MITOL protein in COS-7 and HeLa cell lines. Lysates of COS-7, HeLa and MITOL expression vector-transfected HeLa cells were immunoblotted with control preimmune or immune serum containing anti-MITOL antibody.

In order to examine subcellular distribution of MITOL in HeLa cells, immunohistochemical analysis using anti-MITOL antibody was performed and is shown in Figure 2A (upper panels). Endogenous MITOL was colocalized with mitochondrial marker MitoTracker, suggesting that MITOL is a mitochondrial protein. Likewise, HeLa cells expressing Myc-tagged MITOL were immunostained with anti-Myc antibody and MitoTracker. Myc-tagged MITOL was also colocalized with mitochondria (Figure 2A, lower panels). To confirm the mitochondrial localization of MITOL, cytosolic and mitochondrial fractions of normal HeLa or HeLa cells expressing Myc-tagged MITOL were isolated and MITOL localization was determined by immunoblotting using anti-MITOL (Figure 2B, left) or anti-Myc antibodies (Figure 2B, right). As expected, MITOL was localized in the mitochondrial fraction. As the mitochondrial fraction is known to contain a part of endoplasmic reticulum (ER) proteins, mitochondrial and ER-rich fractions were separated and MITOL localization was examined using anti-PDI (ER marker) and anti-Tom20 antibodies (mitochondria marker). As shown in Figure 2C, MITOL was not detected in the ER-rich fraction, indicating the specific localization of MITOL in mitochondria. Carbonate extraction assay showed that MITOL behaved like an integral membrane protein. This result was consistent with predicted four-transmembrane structure (Figure 2D). We next examined whether MITOL localized at the outer or inner membrane of mitochondria. Purified intact mitochondria prepared from HeLa cells were treated with trypsin, which attacked the cytosolic domain of the outer membrane proteins. Treatment with trypsin did not affect the inner membrane protein Tim23, whereas it degraded MITOL as well as the outer membrane protein Tom20 (Figure 2E). Mitochondrial outer membrane proteins were removed from mitochondria by nonionic detergent digitonin treatment. The digitonin solubility of MITOL was consistent with that of Tom20 but not Tim23 (Figure 2E). To determine the topology of the N-terminus, trypsin protection assay on mitochondria isolated from cells expressing an N-terminally HA-tagged MITOL was performed. As shown in Figure 2E (right panel), the N-terminal PHD domain rapidly disappeared from mitochondria by trypsin treatment. These results suggested that MITOL was localized at mitochondrial outer membranes and the N-terminal PHD domain is exposed to the cytoplasm.

Rapid degradation of MITOL by autoubiquitination activity

To understand the metabolic steady-state level of MITOL expression, the effect of protein synthesis inhibitor cycloheximide (CHX) on MITOL expression was examined. As shown in Figure 3A (left panel), CHX treatment downregulated MITOL expression and this was blocked by addition of proteasome inhibitor MG132. A similar result was obtained

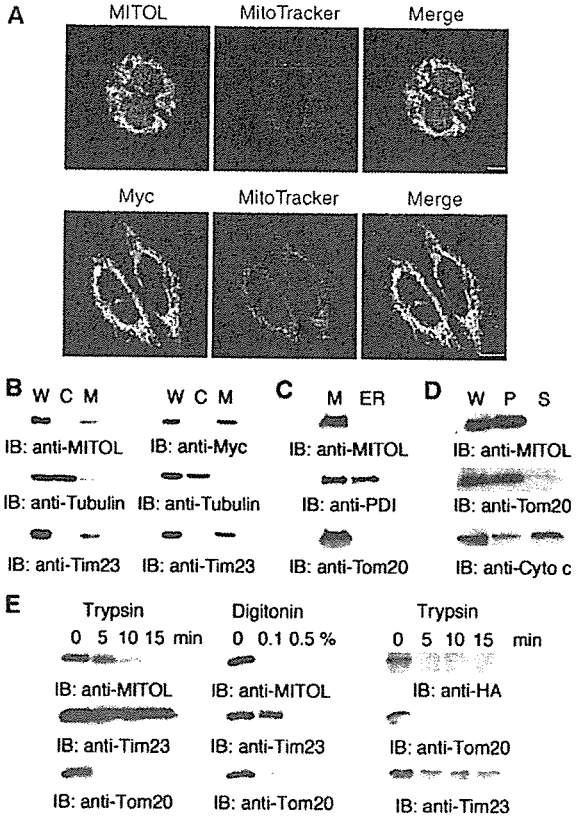

Figure 2 Specific localization of MITOL in the outer mitochondrial membrane. (**A**) Colocalization of MITOL with mitochondria. (Upper panels) HeLa cells were immunostained with anti-MITOL (green) antibody and MitoTracker (red). (Lower panels) HeLa cells expressing Myc-tagged MITOL were immunostained with anti-Myc antibody (green) and MitoTracker (red). (**B**) Subcellular fractionation indicates the localization of MITOL in mitochondria. Whole lysates (W) and cytosolic (C) and mitochondrial fractions (M) isolated from HeLa (left) or HeLa cells expressing Myc-MITOL (right) were immunoblotted with anti-MITOL, anti-Myc, anti-tubulin or anti-Tim23 mitochondria marker antibodies. (**C**) MITOL is not localized in ER. The mitochondrial fraction (M) and the ER-rich fraction (ER) isolated from HeLa cells were immunoblotted with anti-MITOL, anti-PDI (ER marker) or anti-Tom20 (mitochondria marker) antibodies. (**D**) Carbonate extraction assay indicates that MITOL is an integral membrane protein. Whole lysates (W), supernatant (S; peripheral protein) and pellet (P; integral protein) fractions after carbonate extraction from isolated mitochondria were immunoblotted with anti-MITOL, anti-Tom20 or anti-cytochrome *c* antibodies. (**E**) Sensitivity of MITOL to trypsin or digitonin treatment indicates MITOL localization in the mitochondrial outer membrane. Purified mitochondria from HeLa cells (left and middle panels) or cells expressing an N-terminally HA-tagged MITOL (right panel) were treated with trypsin or digitonin, and disappearance of MITOL along with mitochondrial markers was monitored by immunoblotting with anti-MITOL, anti-HA, anti-Tim23 or anti-Tom20 antibodies.

in HeLa cells expressing FLAG-MITOL (Figure 3A, right panel). The half-life of FLAG-MITOL was about 60 min and it became difficult to detect the MITOL protein band after 3 h treatment with CHX. On the other hand, treatment with MG132 blocked the CHX-induced downregulation of MITOL (lane 7). Equal amount of tubulin staining demonstrated that the same amount of protein was loaded in each lane. Compared to FLAG-MITOL, endogenous MITOL showed a slow degradation after CHX treatment, suggesting that endogenous MITOL may be regulated by an unknown modification.

To determine whether ubiquitin ligase activity in MITOL-PHD was required for this degradation of MITOL, the effect of CHX treatment on the degradation of CS mutant was similarly studied. Figure 3B shows that CHX treatment failed to degrade the CS mutant. This suggested that the degradation of MITOL was PHD-dependent. We therefore investigated whether MITOL exhibited autoubiquitination activity. Immunoprecipitation of FLAG-MITOL with anti-FLAG antibody from HeLa cells coexpressing FLAG-MITOL and HA-ubiquitin revealed significant polyubiquitination of FLAG-MITOL wild type (WT) but not CS mutant (Figure 3C). This result indicated that MITOL has an autoubiquitination activity. Taken together, these results suggested that MITOL strictly controls its protein expression level by rapid degradation of MITOL through the PHD-dependent autoubiquitination activity.

To investigate the physiological relevance of this rapid turnover of MITOL by autoubiquitination activity, the effects of CS mutant on mitochondrial function and morphology were examined using a transient expression system. We found that compared to MITOL WT, CS mutant significantly induced mitochondrial aggregation (Figure 3D). Statistical analysis showed that over 80% of CS mutant-expressing mitochondria formed aggregates, whereas only 10–20% of WT-expressing mitochondria were aggregated. Western blot analysis indicated an accumulation of CS mutant but not WT in the insoluble fraction of mitochondria (Figure 3E). Electron microscopic analysis revealed the mitochondrial swelling and collapse in CS mutant-expressing cells (Figure 3F). This phenomenon was not observed in WT-expressing mitochondria. This mitochondrial dysfunction may be caused by the accumulation of insoluble or unfolded CS mutant. Taken together, these results suggested that ubiquitin ligase activity of MITOL was necessary for inhibiting accumulation of degenerated MITOL, including other proteins, in mitochondria.

Requirement of MITOL for mitochondrial dynamics through interaction with and ubiquitination of mitochondrial fission factors

To assess the role of MITOL in mitochondria, we established several HeLa cell lines stably expressing FLAG-MITOL WT or FLAG-MITOL CS mutant. We found that the stable expression level of FLAG-MITOL WT or CS mutant was greatly lower than its transient expression (Figure 4A, right panel). This may be owing to the downregulation of FLAG-MITOL through an unknown mechanism to protect cells from toxicity, such as mitochondrial aggregation induced by overexpression of FLAG-MITOL WT or CS mutant. Indeed, no significant mitochondrial aggregation was observed in stable clones of HeLa cell line expressing FLAG-MITOL WT or CS mutant. Instead, HeLa cell lines expressing CS mutant (but not WT) frequently showed an abnormal mitochondrial morphology, such as fragmentation (Figure 4A, left panel). About 30–50% of mitochondria in CS mutant cell line revealed mitochondrial fragmentation. Other two CS mutants also showed a similar mitochondrial fragmentation. To verify this phenomenon, the effects of MITOL knockdown on mitochondrial morphology were examined. HeLa cells transfected with scramble small interfering RNA (siRNA) as control or two siRNAs against

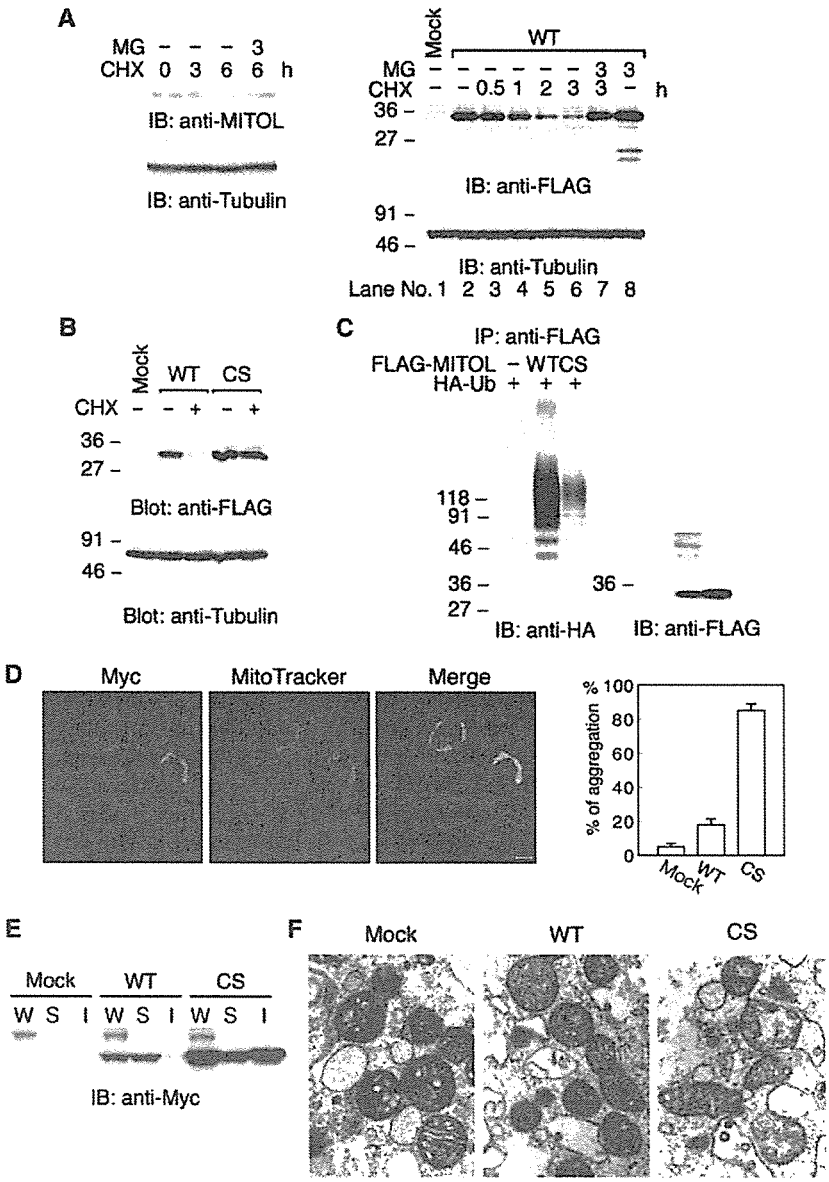

Figure 3 Rapid degradation of MITOL by autoubiquitination activity. (**A**) Effect of protein synthesis inhibitor CHX on MITOL protein expression. HeLa cells (left panel) or HeLa cells expressing FLAG-MITOL WT (right panel) were treated with or without CHX (10 μg/ml) for indicated times in the presence or absence of MG132 (50 μM) and cell lysates were immunoblotted with anti-MITOL, anti-FLAG or anti-tubulin antibodies. (**B**) No degradation of MITOL CS mutant. HeLa cells or HeLa cells expressing FLAG-MITOL WT or FLAG-MITOL CS mutant were treated with or without CHX (10 μg/ml) for 3 h and immunoblotted with anti-FLAG or anti-tubulin antibodies. (**C**) Polyubiquitination of MITOL WT but not MITOL CS mutant. Lysates of HeLa cells cotransfected with control vector, FLAG-MITOL WT or FLAG-MITOL CS mutant with HA-tagged ubiquitin (HA-Ub) were immunoprecipitated with anti-FLAG antibody agarose beads and immunoblotted with anti-HA or anti-FLAG antibodies. (**D**) Mitochondrial aggregation by MITOL CS mutant. HeLa cells expressing Myc-MITOL WT and CS mutant were stained with anti-Myc antibody and MitoTracker. Bar, 10 μm. Mitochondrial aggregation induced by MITOL WT or CS mutant was measured by counting at least 100 cells (right panel). Error bars represent s.d. $n = 3$. (**E**) Accumulation of MITOL CS mutant in the insoluble fraction. Whole lysates (W) and soluble (S) and insoluble (I) fractions were isolated from HeLa cells or HeLa cells expressing Myc-MITOL WT or CS mutants and immunoblotted with anti-Myc antibody. Bars, 10 μm. (**F**) Electron microscopic analysis indicated severe mitochondrial damage in MITOL CS mutant-overexpressing cells. Mitochondrial morphology in control vector, MITOL WT or CS mutant-transfected cells was examined by electron microscopic analysis at 27 600-fold magnification.

MITOL were incubated for 48 h and the expression level of endogenous MITOL was monitored by immunoblot analysis probed with anti-MITOL antibody. As shown in Figure 4B, both the siRNAs against MITOL, but not scramble, reduced MITOL expression by about 70–90%. Using this system, we compared the mitochondrial morphology between control and MITOL-deficient mitochondria and found an increase in mitochondrial fragmentation in MITOL-deficient mitochondria. Statistical analysis showed that over 50% of mitochondria were fragmented in cells transfected with siRNA1 or siRNA2. We generated other three siRNAs against MITOL and found that cells transfected with these three siRNAs showed a

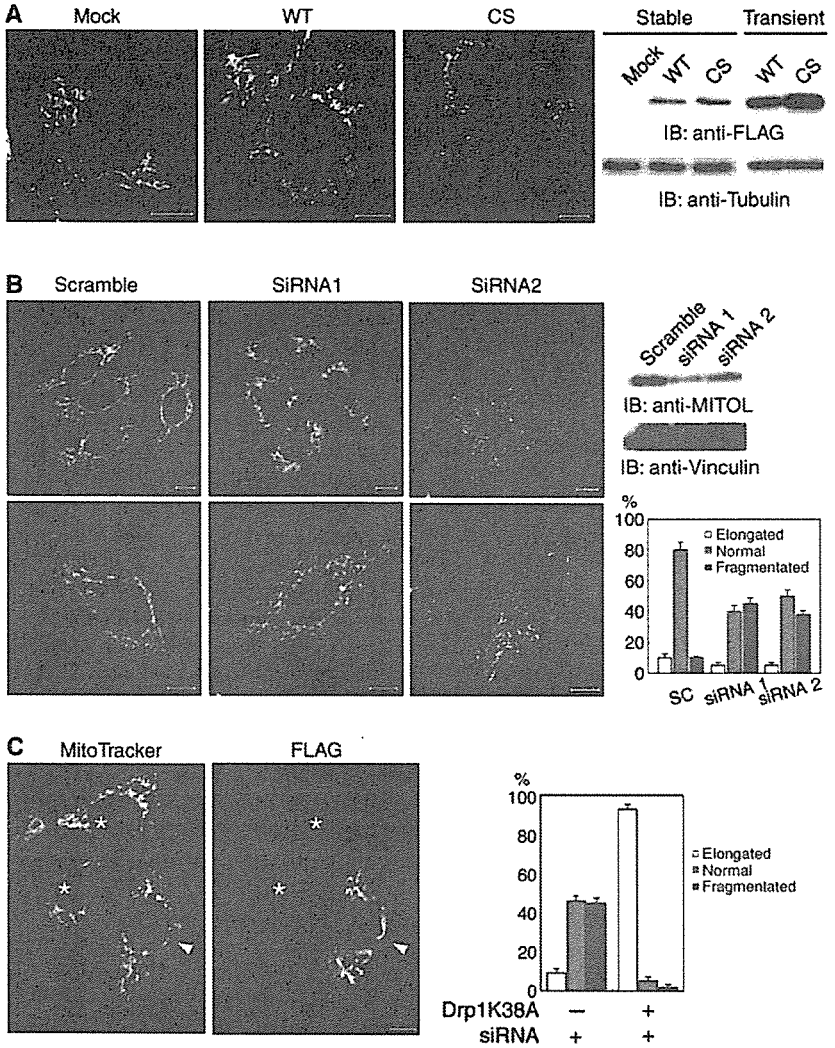

Figure 4 Critical role of MITOL in mitochondrial morphology. (**A**) Mitochondrial fragmentation in HeLa cell lines stably expressing FLAG-MITOL CS mutant. HeLa cell lines stably expressing control vector, FLAG-MITOL WT or CS mutant were stained with MitoTracker and mitochondrial morphologies were compared. The expression levels of FLAG-MITOL after stable and transient transfection relative to mock-transfected cells were shown by immunoblotting using anti-FLAG antibody (right panel). Bars, 10 μm. (**B**) Aberrant mitochondrial morphology in MITOL-deficient cells. HeLa cells transfected with scramble, MITOL siRNA1 or siRNA2 were immunoblotted with anti-FLAG and anti-vinculin antibodies (right) or stained with MitoTracker (left). Bars, 10 μm. Percentages of cells showing each mitochondrial morphology were calculated from 100 scramble- or MITOL siRNA-transfected cells. Error bars represent s.d. $n = 3$. (**C**) Dominant-negative Drp1 mutant blocked mitochondrial fragmentation by MITOL depletion. HeLa cells transfected with FLAG-Drp1 mutant (K38A) and siRNA1 were stained with MitoTracker and anti-FLAG antibody. An arrowhead and asterisks indicate siRNA1-mediated MITOL-depleted cells with or without Drp1 mutant expression, respectively. Bars, 10 μm. Percentages of cells showing each mitochondrial morphology were calculated from 100 MITOL-depleted cells with or without Drp1 mutant expression. Error bars represent s.d. $n = 3$.

similar mitochondrial fragmentation (not shown). This result suggested the enhancement of mitochondrial fission by MITOL depletion. To determine whether mitochondrial fragmentation caused by overexpression of siRNA-mediated depletion of endogenous MITOL is specific to hFis1/Drp1-dependent fission, we examined the effect of dominant-negative Drp1 GTPase-deficient mutant (Drp1K38A) expression on the MITOL-deficient mitochondrial morphology. As shown in Figure 4C, after cotransfection of siRNA and Drp1K38A, the dominant-negative Drp1 mutant blocked mitochondrial fragmentation by siRNA1-mediated MITOL depletion. Statistical analysis demonstrated that Drp1 mutant induced mitochondrial elongation in over 90% of MITOL-depleted cells. These results indicated that MITOL was required for normal mitochondrial morphology and was involved in mitochondrial dynamics probably through the regulation of mitochondrial fission.

Experiments with siRNA-mediated knockdown of MITOL suggested that mitochondrial fission factors such as hFis1 or Drp1 may be substrate for MITOL. To explore this possibility, we investigated whether MITOL could ubiquitinate hFis1. As shown in Figure 5, MITOL WT, but not CS mutant, was found to ubiquitinate hFis1. In addition, co-immunoprecipitation assay revealed that MITOL associated with hFis1 (Figure 5B). To examine the role of MITOL in the control of endogenous hFis1, adenovirus-based constructs expressing MITOL WT

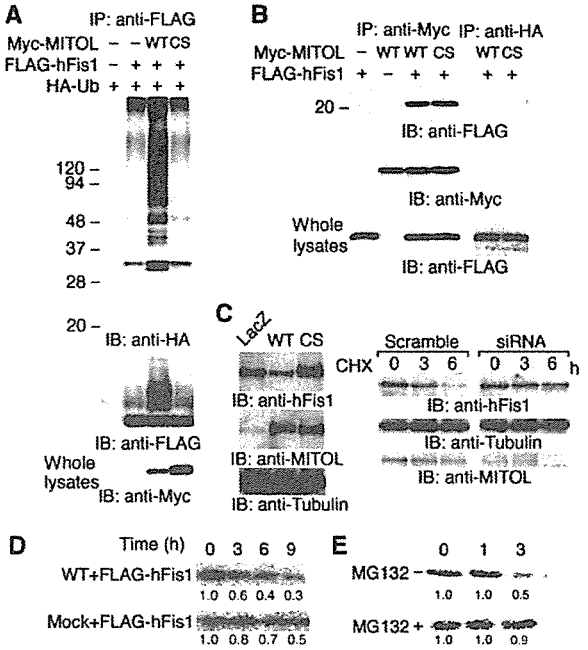

Figure 5 MITOL associates with and ubiquitinates mitochondrial fission protein hFis1. (**A**) Ubiquitination of hFis1 by MITOL. Lysates of HeLa cells transfected with indicated vectors were immunoprecipitated with anti-FLAG antibody and immunoprecipitates were immunoblotted with anti-HA or anti-FLAG antibodies. Whole lysates were immunoblotted with anti-Myc antibody. (**B**) Interaction of MITOL with hFis1. Lysates of HeLa cells transfected with indicated vectors were immunoprecipitated with anti-Myc antibody and immunoprecipitates were immunoblotted with anti-FLAG or anti-Myc antibodies. To demonstrate the specificity of the co-immunoprecipitation, anti-HA antibody was used as a negative control. Whole lysates were immunoblotted with anti-FLAG antibody to confirm the expression of FLAG-hFis1. (**C**) Accumulation of endogenous hFis1 by MITOL dysfunction. Lysates of HeLa cells infected with indicated adenovirus vectors were immunoblotted with anti-hFis1, anti-MITOL or anti-tubulin antibodies (left panel). Lysates of HeLa cells transfected with scramble or MITOL siRNA1 were treated with CHX (10 μg/ml) for indicated times and immunoblotted with anti-hFis1, anti-tubulin or anti-MITOL antibodies (right panel). (**D**) MITOL expression caused a rapid turnover of hFis1. Pulse–chase experiment was performed. HeLa cells expressing FLAG-hFis1 or FLAG-hFis1/MITOL WT were labeled for 60 min with [^{35}S]Met/Cys labeling mixture and chased in complete DMEM for indicated periods. (**E**) Effect of MG132 on hFis1 turnover promoted by MITOL overexpression. HeLa cells expressing FLAG-hFis1/MITOL WT in the absence or presence of MG132 were similarly chased for indicated periods. Cells were lysed and immunoprecipitated with anti-FLAG antibody and immunoprecipitated FLAG-hFis1 was visualized by autoradiography. The result (D or E) is representative of three independent experiments. Relative values estimated by NIH image analysis are indicated below.

and CS mutant were generated. Compared to cells expressing LacZ as control, endogenous hFis1 was decreased in cells expressing MITOL WT. On the other hand, an increase in endogenous hFis1 was detected in cells expressing MITOL CS or MITOL-deficient cells by siRNA1 (Figure 5C). CHX treatment suggested the delayed degradation of endogenous hFis1 in MITOL-deficient cells. To further demonstrate MITOL-dependent turnover of hFis1, pulse–chase experiment was performed. As shown in Figure 5D and E, MITOL overexpression promoted hFis1 turnover and this effect was inhibited by MG132 treatment. Immunoblot analysis probed with anti-FLAG antibody indicated that an equal amount of hFis1 was immunoprecipitated (not shown). Thus, MITOL may control the protein expression level of hFis1 through the ubiquitin–proteasome pathway. Indeed, overexpression of hFis1 causes mitochondrial fragmentation (Figure 6A). Therefore, we next tested whether overexpression phenotype of hFis1 can be reverted by co-overexpression of MITOL. Expectedly, co-overexpression of MITOL WT, but not CS mutant, blocked hFis1-induced mitochondrial fragmentation (Figure 6B and C). Coexpression of MITOL CS mutant induced mitochondrial aggregation consisting of fragmented mitochondria.

Association of Drp1 with MITOL and MITOL-dependent ubiquitination were similarly observed as shown in Supplementary data 1. Pulse–chase experiment also indicated that MITOL overexpression promoted Drp1 turnover. However, ubiquitination of Drp1 by MITOL was lower than that of hFis1 and expression level of endogenous Drp1 was not affected by adenovirus-mediated expression of MITOL WT (not shown). This may be due to the cytosolic distribution of Drp1 compared to mitochondrial membrane localization of hFis1. Alternatively, hFis1 may be better substrate than Drp1 for MITOL. Taken together, these results suggest that MITOL is involved in mitochondrial dynamics through the control of hFis1 and Drp1 by direct interaction and ubiquitination.

Discussion

In this study, we identified a novel membrane-bound ubiquitin ligase designated MITOL, which is specifically localized in mitochondria. As no mitochondria-specific ubiquitin ligase has been reported to date, the discovery of MITOL is a first indication that mitochondria have a putative ubiquitination system. MITOL appeared to be identical to March-V whose function has not been reported except for a description of its ER localization (Bartee *et al*, 2004). In their paper, characterization of March-V localization is very poor and our results indicated that their description about March-V is not correct. Here, we have demonstrated that MITOL is involved in mitochondrial dynamics. A new family of proteins containing PHD motif has been shown to constitute a widely distributed subfamily of zinc-finger proteins that function as E3 ubiquitin ligases. Several PHD-containing viral proteins have been identified that promote immune evasion by downregulating proteins that govern immune recognition (Ishido *et al*, 2000a). Therefore, this family has a common feature to promote or help the survival of certain virus or organelles such as mitochondria in the host cells.

In eukaryotes, mitochondria are dynamic mobile organelles varying in number and shape. The equilibrium between opposing fission and fusion is important for the maintenance of mitochondrial morphologies (Yaffe, 1999; Shaw and Nunnari, 2002). In mammalian cells, the outer membrane protein Fzo1/mitofusin (Chen *et al*, 2003) and the inner membrane protein OPA1 play a role in mitochondrial fusion (Misaka *et al*, 2002), whereas the cytosolic protein Drp1 and the outer membrane protein hFis1 are involved in mitochondrial fission (Smirnova *et al*, 2001; James *et al*, 2003). However, the regulation of the dynamic balance between fission and fusion is largely unknown so far. In yeast, Mdm30, an E3 ubiquitin ligase containing an F-box motif, has been reported to regulate the protein level of Fzo1 (Fritz *et al*, 2003). On the other hand, sumoylation of Drp1

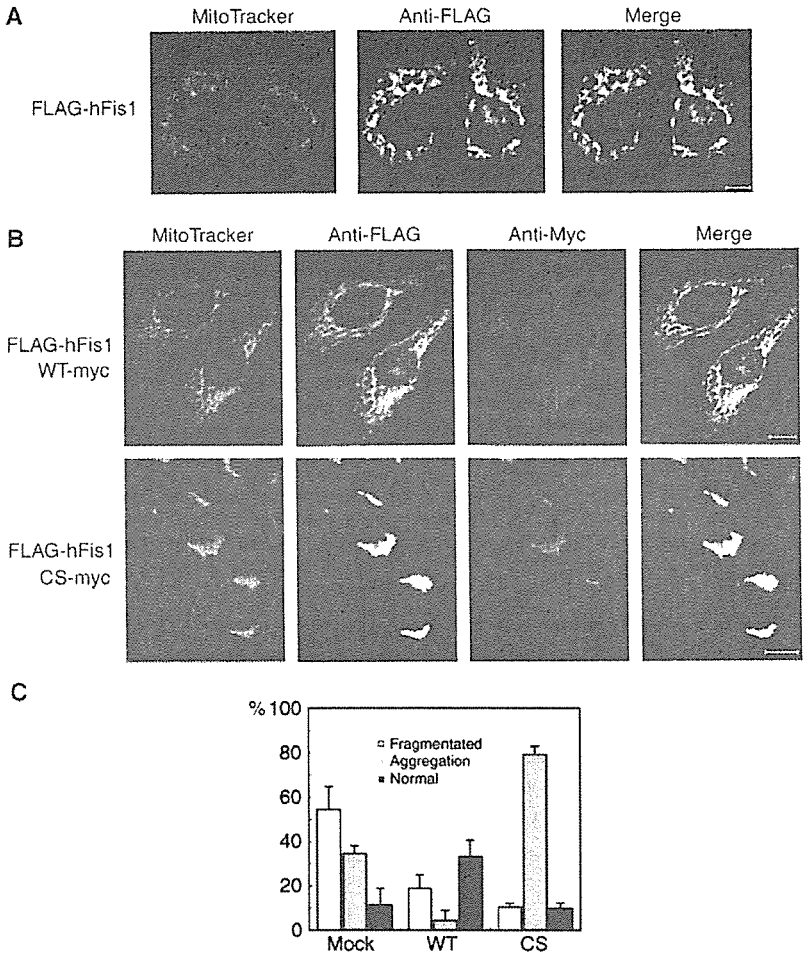

Figure 6 Rescue of hFis1 expression phenotype by MITOL coexpression. (**A**) Mitochondrial fragmentation by hFis1 expression. HeLa cells expressing FLAG-hFis1 were stained with MitoTracker and anti-FLAG antibody. Bars, 10 μm. (**B**) Coexpression of MITOL WT, but not CS mutant, blocked hFis1-induced mitochondrial fragmentation. HeLa cells coexpressing Myc-MITOL WT or CS mutant with FLAG-hFis1 were stained with MitoTracker, anti-FLAG and anti-Myc antibodies. Bars, 10 μm. (**C**) Percentages of cells showing each mitochondrial morphology were calculated from 100 hFis1, hFis1/MITOL WT or hFis1/MITOL CS coexpressing cells. Error bars represent s.d. $n = 3$.

elevates its steady-state level at mitochondria and accelerates mitochondrial fragmentation (Harder *et al*, 2004). Thus, one model to explain how to coordinate the balance between fusion and fission is the control of protein level of these factors involved in fusion and fission by the modification of sumoylation and ubiquitination. Indeed, MITOL-deficient HeLa cells displayed a number of fragmented or very short filamentous mitochondria (Figure 4). Cotransfection and pulse–chase experiments indicated that hFis1 and Drp1 were associated with and ubiquitinated by MITOL. Therefore, MITOL may be closely involved in mitochondrial dynamics via the control of hFis1 and Drp1 protein level through the ubiquitin–proteasome pathway. As mitochondrial fusion factors, as well as fission factors, may also be regulated by MITOL, the relationship between MITOL and fusion factors should be further investigated.

E3 ubiquitin ligases are distributed widely in the cells, including the plasma membrane, cytoplasm, Golgi and ER. In particular, membrane-bound ubiquitin ligases localized at ER have been demonstrated to be involved in the protein quality control through the interaction with chaperone (Sitia and Braakman, 2003). In mitochondria, unfolded proteins have been believed to be degraded by ATP-dependent proteases localized in each compartment in mitochondria (Langer *et al*, 2001; Arnold and Langer, 2002). However, several mitochondrial proteins such as Tom20 and prohibitin have been reported to be ubiquitinated (Wright *et al*, 2001; Thompson *et al*, 2003), suggesting the existence of a specific ubiquitin–proteasome system in mitochondria. As we identified a chaperone as one of MITOL-interacting proteins, it is possible that MITOL interacts with and ubiquitinates unfolded mitochondrial proteins. Mitochondria may possess a putative ubiquitination pathway as a protein quality control system. We are now investigating the role of MITOL in mitochondria quality control.

In our preliminary observation, analysis of time-lapse imaging suggested the severe defect in mitochondrial movement in siRNA-mediated MITOL-depleted cells. In these cells, mitochondria stayed at the same position and often revealed a perinuclear aggregation. Interestingly, one of MITOL-interacting proteins is closely related with motor protein. Thus, MITOL may be involved in the microtubule-based motility of mitochondria. We are currently trying to generate transgenic mice expressing MITOL WT or CS mutant. We have already

succeeded in generating transgenic mice overexpressing MITOL WT, but not CS mutant, suggesting that the transgenic mice expressing MITOL CS mutant may be nonviable. Further study would be necessary for understanding the function of MITOL.

Materials and methods

Database searches and cloning of human MITOL cDNA

For the cloning of cDNA coding human MITOL, total RNA isolated from BJAB cells was reverse-transcribed using the Superscript RT kit (Invitrogen) according to the manufacturer's protocol. To determine the 5′ and 3′ ends of the entire coding sequence of MITOL cDNA, 5′ and 3′ rapid amplification of cDNA ends was performed using a GeneRacer Kit (Invitrogen). A full-length cDNA of MITOL was obtained by PCR and subcloned into the pEF-1 (Invitrogen) and pAAV IRES-EGFP vectors and sequenced using a model 310 DNA sequencer (Applied Biosystems). To introduce C-terminal FLAG and Myc epitope tags, MITOL cDNAs were amplified by PCR using adequate primers and subcloned into pApuro vectors. The putative secondary structure and transmembrane topology of MITOL were examined by profile fed neural network system from Heidelberg (PHD) and sosui program. Point mutations of Cys^{65} and Cys^{68} of MITOL cDNA to Ser were generated by the site-directed mutagenesis kit (Stratagene).

Detection of MITOL mRNA in human tissues

Poly(A) + RNA blots containing 1 μg of poly(A) + RNA per lane from mouse NorthernLIGHT Blots (Panomics) were hybridized with the ^{32}P-labeled full-length mouse MITOL cDNA. Hybridization was carried out according to the manufacturer's protocol. After washing, the membrane was exposed to X-ray film at −70°C using an intensifying screen (Inatome *et al*, 2000).

Cell culture and transfection

HeLa and COS-7 cells were grown in Dulbecco's modified Eagle's medium with 10% fetal bovine serum and 100 U/ml penicillin at 5% CO_2 at 37°C. For transient assays, expression plasmids were transfected using lipofectamine plus (Invitrogen) according to the manufacturer's instructions.

Small interfering RNA

For RNAi assay, sense and antisense oligonucleotides corresponding to the following target sequences were purchased from Dharmacon: 5′-GCTCTATCTATTGGACAG-3′ (No. 1), 5′-TCTTGGGTGGAATTGCGTT-3′ (No. 2). Scramble oligonucleotide was used as a negative control. The annealed siRNA duplex was transfected into HeLa cells using Lipofectamine 2000 (Invitrogen).

Antibodies

Antibody directed against MITOL was produced by immunizing rabbits with a synthetic peptide, GCKQQQYLRQAHRKILNYPEQEEA, corresponding to amino acids 257–279 of MITOL. Anti-FLAG (M2), anti-α-tubulin and anti-vinculin antibodies were from Sigma. Anti-c-Myc antibody was from Roche. Anti-HA antibody was from Babco. Anti-ubiquitin (P4D1) antibody was from Santa Cruz. The mouse monoclonal antibodies against cytochrome *c*, Tom20, Tim23 and PDI were purchased from BD Biosciences.

Immunofluorescence microscopy

Cells were fixed with 4% paraformaldehyde in phosphate-buffered saline (PBS) for 1 h at 37°C, then washed twice with 0.2% Tween 20 in PBS, permeabilized with 0.2% Triton X-100 in PBS for 10 min, washed four times with PBS and blocked with 3% bovine serum albumin in PBS, all at room temperature. For double staining, the cells were incubated with appropriate primary antibodies for 1 h at room temperature, washed three times with 0.5% Triton X-100 in PBS and then with appropriate secondary antibodies (Alexa Fluor goat anti-rabbit IgG, Alexa Fluor goat anti-mouse IgG) for 30 min. To visualize the mitochondria, 100 nM MitoTracker (Molecular Probes) was added and incubated for 30 min. The samples were washed as before, mounted using PermaFluor (Immunon) and analyzed using Zeiss LSM510 confocal laser scanning microscope (Hotta *et al*, 2005).

Electron microscopic analysis

HeLa cells expressing MITOL WT or CS mutant were fixed with 2.5% glutaraldehyde in 0.1 M sodium phosphate buffer (pH 7.4). They were postfixed with 2% OsO_4 in the same buffer. After dehydration with a graded series of ethanol, they were substituted by propylene oxide and embedded in Epoxy resin. Silver to gold thin sections were doubly stained with uranyl acetate and lead citrate, and examined with an H-7000 transmission electron microscope (Hitachi, Tokyo, Japan) and photographed at various magnifications.

Immunoprecipitation and immunoblotting

Preparation of cell lysates, immunoprecipitation and immunoblotting were performed as described previously (Kyo *et al*, 2003). To investigate the ubiquitination of proteins, cells were solubilized in lysis buffer (1% Triton X-100, 50 mM Tris, pH 7.4, 150 mM NaCl, 10 mM EDTA, 1 mM PMSF, 2 μg/ml aprotinin) to dissociate protein complexes. Total cell lysates were prepared by the direct addition of 1 × SDS sample buffer to the monolayers. Immunoprecipitates and total cell lysates were separated by SDS–PAGE and transferred to the PVDF membrane (Millipore) (Mitsui *et al*, 2002). The blots were probed with the indicated antibodies. In all blots, proteins were visualized by the enhanced chemiluminescence reagent (Western Lightning; PerkinElmer LifeScience).

Plasmid construction

Drp1 cDNA with C-terminal FLAG epitope tag and hFis1 with N-terminus were obtained from total RNA of HeLa cells by RT–PCR and subcloned into pCMV5 expression vector. Point mutations of Lys^{38} of Drp1 cDNA to Ala were generated by the site-directed mutagenesis. To construct plasmid DNAs for GST fusion proteins, a fragment encoding MITOL PHD domain was amplified by PCR and then subcloned into pGEX 4T-3 vector (Amersham Biosciences).

Subcellular fractionation

Isolation of mitochondria was performed using a mitochondrial fractionation kit (Active Motif). The supernatant and pellets collected were used as ER and mitochondrial fractions, respectively. Protein concentration was measured using a Bio-Rad protein assay (Bio-Rad) with BSA as a standard.

Carbonate extraction assay

To confirm whether MIOL is peripheral protein or integral protein, we performed carbonate extraction. Mitochondrial suspensions in isotonic buffer (250 mM sucrose, 2.5 mM Hepes pH 7.5) were added with an equal volume of 200 mM Na_2CO_3 (pH 11.5) (final 100 mM) and incubated on ice for 30 min. The suspensions were centrifuged at 144 000*g* at 4°C for 1 h. The supernatant (peripheral protein fraction) and the pellets (integral protein fraction) collected were diluted with 100 mM Na_2CO_3 in isotonic buffer.

Pulse–chase analysis

HeLa cells were incubated for 1 h with Met/Cys-free DMEM followed by addition of 500 μCi ^{35}S-labeled Met/Cys mixture for 1 h. Following labeling, cells were washed in PBS and incubated in complete medium without radioactive amino acids for the indicated times. Cells were washed in PBS, lysed and equal protein amounts subjected to immunoprecipitation with anti-FLAG M2 agarose (Sigma).

Ubiquitination assay

For *in vitro* autoubiquitination assay, GST fusion proteins were produced as follows. Expression of GST fusion proteins was induced by 0.1 mM isopropyl-1-D-thio-galactopyranoside for 3–6 h. Bacterial pellets were sonicated in 1% Triton X-100 lysis buffer containing protease inhibitors. After being cleared by centrifugation, bacterial lysates were incubated with glutathione-Sepharose beads (Amersham Biosciences). A 10 μg portion of precipitated GST fusion protein was washed three times with lysis buffer, once with ubiquitination buffer (40 mM Tris–HCl, pH 7.5, 5 mM $MgCl_2$, 2 mM ATP, 2 μM dithiothreitol, 25 μM MG132) and incubated in 150 μl of the same buffer supplemented with rabbit reticulocytes lysate and 40 μg of His-tagged ubiquitin (Calbiochem) for 2 h at 30°C. After *in vitro* ubiquitination, all samples were washed four times with lysis buffer, eluted with SDS-sample buffer and subjected to immunoblot analysis by probing with anti-ubiquitin (P4D1) antibody.

Adenovirus-based vector construction

The adenovirus-based MITOL vectors were generated by the ViraPower Adenoviral Gateway Expression (Invitrogen). 293T cells were transfected with the recombinant adenoviral plasmid using lipofectin (Invitrogen), and adenovirus with the titer of 10^{10}–10^{12} PFU/ml was collected.

Digitonin/trypsin treatment

Isolated mitochondria were diluted with mitochondrial buffer (70 mM sucrose, 220 mM D-mannitol, 2.5 mM Hepes-KOH pH 7.4) and digitonin was added at a final concentration of 0, 0.1 or 0.5% (w/v). Each sample was incubated on ice for 10 min and added 4 volumes of mitochondrial buffer and centrifuged at 11 000 r.p.m. at 4°C for 10 min. Each pellet was suspended with mitochondrial buffer and analyzed by Western blot. For trypsin treatment, trypsin was added to the mitochondrial fraction at a final concentration of 1% and incubated on ice for 0, 5, 10 or 15 min. After addition of protease inhibitor and centrifugation at 11 000 r.p.m. at 4°C for 10 min, each pellet was suspended with mitochondrial buffer and analyzed by Western blot.

Supplementary data

Supplementary data are available at *The EMBO Journal* Online.

Acknowledgements

This study was supported in part by grants-in-aid for scientific research from MEXT and JSPS. We are grateful to Mr T Kozaki for technical assistance. We thank Dr D Bohmann for the HA-ubiquitin expression plasmid and Dr H Hirai for the pAAV IRES-EGFP vector. We also thank Dr S Jahangeer and Dr M Kojima for critical reading of the manuscript.

References

Arnold I, Langer T (2002) Membrane protein degradation by AAA proteases in mitochondria. *Biochim Biophys Acta* **1592:** 89–96

Bartee E, Mansouri M, Hovey Nerenberg BT, Gouveia K, Fruh K (2004) Downregulation of major histocompatibility complex class I by human ubiquitin ligases related to viral immune evasion proteins. *J Virol* **78:** 1109–1120

Chen H, Detmer SA, Ewald AJ, Griffin EE, Fraser SE, Chan DC (2003) Mitofusins Mfn1 and Mfn2 coordinately regulate mitochondrial fusion and are essential for embryonic development. *J Cell Biol* **160:** 189–200

Coscoy L, Ganem D (2003) PHD domains and E3 ubiquitin ligases: viruses make the connection. *Trends Cell Biol* **13:** 7–12

Fritz S, Weinbach N, Westermann B (2003) Mdm30 is an F-box protein required for maintenance of fusion-competent mitochondria in yeast. *Mol Biol Cell* **14:** 2303–2313

Goto E, Ishido S, Sato Y, Ohgimoto S, Ohgimoto K, Nagano-Fujii M, Hotta H (2003) c-MIR, a human E3 ubiquitin ligase, is a functional homolog of herpesvirus proteins MIR1 and MIR2 and has similar activity. *J Biol Chem* **278:** 14657–14668

Griparic L, van der Bliek AM (2001) The many shapes of mitochondrial membranes. *Traffic* **2:** 235–244

Hales KG, Fuller MT (1997) Developmentally regulated mitochondrial fusion mediated by a conserved, novel, predicted GTPase. *Cell* **90:** 121–129

Harder Z, Zunino R, McBride H (2004) Sumo1 conjugates mitochondrial substrates and participates in mitochondrial fission. *Curr Biol* **14:** 340–345

Hermann GJ, Thatcher JW, Mills JP, Hales KG, Fuller MT, Nunnari J, Shaw JM (1998) Mitochondrial fusion in yeast requires the transmembrane GTPase Fzo1p. *J Cell Biol* **143:** 359–373

Hershko A, Ciechanover A (1992) The ubiquitin system for protein degradation. *Annu Rev Biochem* **61:** 761–807

Hershko A, Ciechanover A (1998) The ubiquitin system. *Annu Rev Biochem* **67:** 425–479

Hotta A, Inatome R, Yuasa-Kawada J, Qin Q, Yamamura H, Yanagi S (2005) Critical role of CRMP-associated molecule CRAM for Filopodia and growth cone development in neurons. *Mol Biol Cell* **16:** 32–39

Inatome R, Tsujimura T, Hitomi T, Mitsui N, Hermann P, Kuroda S, Yamamura H, Yanagi S (2000) Identification of CRAM, a novel unc-33 gene family protein that associates with CRMP3 and protein-tyrosine kinase(s) in the developing rat brain. *J Biol Chem* **275:** 27291–27302

Ishido S, Choi JK, Lee BS, Wang C, DeMaria M, Johnson RP, Cohen GB, Jung JU (2000a) Inhibition of natural killer cell-mediated cytotoxicity by Kaposi's sarcoma-associated herpesvirus K5 protein. *Immunity* **13:** 365–374

Ishido S, Wang C, Lee BS, Cohen GB, Jung JU (2000b) Downregulation of major histocompatibility complex class I molecules by Kaposi's sarcoma-associated herpesvirus K3 and K5 proteins. *J Virol* **74:** 5300–5309

Jackson PK, Eldridge AG, Freed E, Furstenthal L, Hsu JY, Kaiser BK, Reimann JD (2000) The lore of the RINGs: substrate recognition and catalysis by ubiquitin ligases. *Trends Cell Biol* **10:** 429–439

James DI, Parone PA, Mattenberger Y, Martinou JC (2003) hFis1, a novel component of the mammalian mitochondrial fission machinery. *J Biol Chem* **278:** 36373–36379

Jensen RE, Hobbs AE, Cerveny KL, Sesaki H (2000) Yeast mitochondrial dynamics: fusion, division, segregation, and shape. *Microsc Res Tech* **51:** 573–583

Kyo S, Sada K, Qu X, Maeno K, Miah SM, Kawauchi-Kamata K, Yamamura H (2003) Negative regulation of Lyn protein-tyrosine kinase by c-Cbl ubiquitin-protein ligase in Fc varepsilon RI-mediated mast cell activation. *Genes Cells* **8:** 825–836

Labrousse AM, Zappaterra MD, Rube DA, van der Bliek AM (1999) *C. elegans* dynamin-related protein DRP-1 controls severing of the mitochondrial outer membrane. *Mol Cell* **4:** 815–826

Langer T, Kaser M, Klanner C, Leonhard K (2001) AAA proteases of mitochondria: quality control of membrane proteins and regulatory functions during mitochondrial biogenesis. *Biochem Soc Trans* **29:** 431–436

Means RE, Ishido S, Alvarez X, Jung JU (2002) Multiple endocytic trafficking pathways of MHC class I molecules induced by a Herpesvirus protein. *EMBO J* **21:** 1638–1649

Misaka T, Miyashita T, Kubo Y (2002) Primary structure of a dynamin-related mouse mitochondrial GTPase and its distribution in brain, subcellular localization, and effect on mitochondrial morphology. *J Biol Chem* **277:** 15834–15842

Mitsui N, Inatome R, Takahashi S, Goshima Y, Yamamura H, Yanagi S (2002) Involvement of Fes/Fps tyrosine kinase in semaphorin3A signaling. *EMBO J* **21:** 3296–3306

Patterson C (2002) A new gun in town: the U box is a ubiquitin ligase domain. *Sci STKE* **2002:** PE4

Pickart CM (2001) Mechanisms underlying ubiquitination. *Annu Rev Biochem* **70:** 503–533

Sesaki H, Jensen RE (1999) Division versus fusion: Dnm1p and Fzo1p antagonistically regulate mitochondrial shape. *J Cell Biol* **147:** 699–706

Shaw JM, Nunnari J (2002) Mitochondrial dynamics and division in budding yeast. *Trends Cell Biol* **12:** 178–184

Sitia R, Braakman I (2003) Quality control in the endoplasmic reticulum protein factory. *Nature* **426:** 891–894

Smirnova E, Griparic L, Shurland DL, van der Bliek AM (2001) Dynamin-related protein Drp1 is required for mitochondrial division in mammalian cells. *Mol Biol Cell* **12:** 2245–2256

Thompson WE, Ramalho-Santos J, Sutovsky P (2003) Ubiquitination of prohibitin in mammalian sperm mitochondria: possible roles in the regulation of mitochondrial inheritance and sperm quality control. *Biol Reprod* **69:** 254–260

Wright G, Terada K, Yano M, Sergeev I, Mori M (2001) Oxidative stress inhibits the mitochondrial import of preproteins and leads to their degradation. *Exp Cell Res* **263:** 107–117

Yaffe MP (1999) The machinery of mitochondrial inheritance and behavior. *Science* **283:** 1493–1497

Journal of Clinical Pharmacy and Therapeutics (2006) **31**, 441–446

ORIGINAL ARTICLE

2′-,5′-Oligoadenylate synthetase response ratio predicting virological response to PEG-interferon-α2b plus ribavirin therapy in patients with chronic hepatitis C

K.-I. Kim* BS, S.-R. Kim† PhD, N. Sasase* MS, M. Taniguchi‡ BS, S. Harada* BS, K. Kinoshita* MS, S.-H. Kim* BS, Y. Akimoto* MS, M. Shikata* BS, N. Kimura* BS, S. Izawa* BS, A. Ohtani* MS, K. Nakao* BS, M. Motojima§ BS, M. Kinoshita§ BS, M. Hirai§ PhD, M. Ohzu¶ BS, T. Hirooka¶ BS, S. Nabeshima¶ BS, F. Ishii¶ MS, K. Tanaka¶ PhD and H. Hotta** PhD

**Department of Pharmacy, Kobe Asahi Hospital, Kobe, Japan, †Department of Gastroenterology, Kobe Asahi Hospital, Kobe, Japan, ‡Medical Information Center, Kobe Asahi Hospital, Kobe, Japan, §Faculty of Pharmaceutical Sciences, Kobe Pharmaceutical University Kobe, Japan, ¶Clinical Pharmacy and Clinical Pharmacokinetics, Osaka University of Pharmaceutical Sciences, Osaka, Japan and **Department of Microbiology, Kobe University Graduate School of Medicine, Kobe, Japan*

SUMMARY

Objective: **Although all the mechanisms of elimination of hepatitis C virus (HCV) by Interferon (IFN) have not been fully elucidated, the 2′-5′-oligoadenylate (2-5A) system is one of the mechanisms of the antiviral effect of IFN. Consequently, the measurement of 2′-5′-oligoadenylate synthetase (2-5AS) activity could be useful for the evaluation of IFN treatment. This retrospective study was aimed at assessing whether 2-5AS activity functions as a clinical marker of virological response to PEG-interferon-α2b (PEG-IFN) plus ribavirin therapy of chronic hepatitis C.**

Methods: **The 32 patients included in this study had high viral loads of serum HCV-RNA of genotype 1b with chronic hepatitis C. All the patients received a regimen of PEG-IFN plus ribavirin for 48 weeks, and were then divided into two groups: one group (effective group) with undetectable serum HCV-RNA levels at 24 weeks (n = 22) of therapy, the other group (ineffective group) with persistent presence of HCV-RNA in serum at 24 weeks (n = 10). The 2-5AS activity in serum was measured 2, 8 and 12 weeks before initial administration.**

Results: **The 2-5AS response ratio (measured value/measured value of baseline 2-5AS) at 2, 8 and 12 weeks after the administration in the effective group was significantly higher than that in the ineffective group.**

Conclusions: **These results suggest that the ratio of 2-5AS is closely related to the antiviral effect, and that the measurement of 2-5AS response ratio may be a useful clinical parameter of virological response to PEG-IFN plus ribavirin therapy of chronic hepatitis C.**

Keywords: **2′,5′-oligoadenylate synthetase, chronic hepatitis C, PEG-interferon-α2b, ribavirin**

INTRODUCTION

Interferon (IFN) treatment is the effective, standard method used worldwide for chronic hepatitis C. However, the effect of IFN administration is limited by several factors, including hepatitis C virus (HCV) genotype, viral load, liver fibrosis and host immunological factors (1, 2). The eradication rate of IFN monotherapy is low (<10%), especially in patients with chronic hepatitis C of genotype 1b and a high viral load (3, 4). To overcome this low

Received 23 April 2006, Accepted 30 May 2006
Correspondence: S.-R. Kim, Department of Gastroenterology, Kobe Asahi Hospital, 3-5-25, Bououji-cho, Nagata-ku, Kobe 653-0801 Hyogo, Japan. Tel.: 81 78 612 5151; fax: 81 78 612 5152; e-mail: info@kobe-asahi-hp.com